Gondwana Research 78 (2020) 291–307

Contents lists available at ScienceDirect

Gondwana Research

journal homepage: www.elsevier.com/locate/gr

Magmatic recycling of accretionary wedge: A new perspective on Silurian-Devonian I-type granitoids generation in the Chinese Altai

Yanqiong Huang [a, b], Yingde Jiang [a, *], Stephen Collett [c], Sheng Wang [a, b], Kang Xu [a, b], Tan Shu [a, b], Pengfei Li [a], Chao Yuan [a]

[a] State Key Laboratory of Isotope Geochemistry, Guangzhou Institute of Geochemistry, Chinese Academy of Sciences, Guangzhou 510640, China
[b] University of Chinese Academy of Sciences, Beijing 100049, China
[c] Center for Lithospheric Research, Czech Geological Survey, Prague, Czech Republic

ARTICLE INFO

Article history:
Received 19 January 2019
Received in revised form
1 July 2019
Accepted 28 July 2019
Available online 10 September 2019

Handling Editor: A. Festa

Keywords:
Anatexis
Volcanogenic sediments
I-type granitoids
Chinese Altai
Continental stabilization

ABSTRACT

The mechanism for generation of Silurian-Devonian hornblende-bearing I-type granitoids in the Chinese Altai still remains rather obscure. The possibility that they are derived from the regional anatexis of the Ordovician accretionary wedge, i.e., the Habahe Group, is investigated. The Habahe Group contains a large number of intermediate-to-basic components. These components occur mainly as interlayered volcanogenic bands or admixtures and less commonly as blocks varying in size from several meters to several hundreds of meters. Geochemically, this volcanogenic component is characterized by enrichment of large-ion lithophile elements relative to many of the high-field strength elements and rather radiogenic Nd isotopic signatures ($\varepsilon_{Nd}(t)$: +4.1 to +9.1). Phase equilibrium and trace element modelling indicate that partial melting of the volcanogenic component at an attainable 900–1000 °C can produce 30–35 vol% silicic melts that show a good chemical match, in terms of major element contents and trace element patterns, with those of the local I-type granitoids. Combined with regional available data, we suggest that Silurian-Devonian hornblende-bearing I-type granitoids could be derived from the partial melting of the volcanogenic components of the Habahe Group and previously inferred large input of mantle-derived magma is un-necessary. Regional anatexis of the Ordovician accretionary wedge led to the stabilization of the wedge, which may represent an important mechanism contributing to the formation of vertically stratified continental crust in accretionary orogens in general.

1. Introduction

The formation of large silicic batholiths, dominantly composed of calc-alkalic granodioritic to tonalitic compositions (I-type granitoid), is classically interpreted as the most conspicuous features of arc magmatism on an active continental margin (Wyllie, 1977), as best exemplified by Cordilleran-type granitoids (Condie, 1997; Hawkesworth et al., 2010). On the one hand, the broadly metaluminous or weakly peraluminous features of this type of granitoids were thought to chemically image their source rocks, and this has led many to suggest that they are generally derived from (meta) igneous rocks rather than sedimentary ones (Chappell et al., 2012; Rutter and Wyllie, 1988; Wolf and Wyllie, 1994). One preferred model invokes extensive fractionation of basaltic magma or partial melting of meta-igneous rocks at deep crustal levels (Annen et al., 2006; Lee and Bachmann, 2014). On the other hand, these I-type granitoid batholiths usually have hybrid mantle-crust geochemical signatures, as evidenced by their variable Sr and Nd isotopic compositions (Allègre and Othman, 1980; DePaolo, 1981; McCulloch and Gamble, 1991), implying significant crust-mantle interaction involved in their generation. Alternatively, numerous experimental and numerical studies postulated that melting of a compositionally heterogeneous source, such as subducted mélanges, is another process capable of generating I-type granitoid batholiths (Annen et al., 2006; Castro et al., 2010; Gerya et al., 2006; Gorczyk et al., 2007; Kruk, 2015). It seems a general consensus that the formation of I-type batholiths is a major contribution to the growth of continental crust (Kemp et al., 2007). Therefore, to decipher the petrogenesis of these rocks is crucial to our understanding of the mechanism for generation and evolution of continental crust.

Pacific-type convergent margins are characterized by long-lasting, continuous subduction of oceanic crust, and are responsible for the sites of major growth of continental lithosphere in areas known as accretionary orogenic belts (Cawood et al., 2009).

* Corresponding author.
E-mail address: jiangyd@gig.ac.cn (Y. Jiang).

https://doi.org/10.1016/j.gr.2019.07.019
1342-937X/

On the one hand, continental crust could form via arc magmatism, through which originally basaltic melts rise, fractionate, crystallize and form mature continental crust (Rudnick, 1995; Solano et al., 2012; Taylor, 1967). On the other hand, the volume of continental crust can be enlarged via accretion of exotic crustal components attached to the host continent, and stratified continental crust could be generated via late magmatic and/or metamorphic reworking (Jiang et al., 2016; Safonova, 2017). The Central Asian Orogenic Belt (CAOB), the largest known crustal growth area during the Phanerozoic on Earth, is composed of various lithological units (Şengör et al., 1993; Wilhem et al., 2012). On the basis of the primitive whole-rock Sr-Nd isotopic characteristics of numerous granitoids, it has been suggested that half of the CAOB crust is juvenile (Jahn et al., 2000; Kröner et al., 2007; Şengör et al., 1993; Xiao et al., 2004, 2009). Genetic models proposed for the formation of juvenile crust in the CAOB varied from the extraction of mantle melts via either arc magmatism (Şengör et al., 1993) or magmatic underplating (e.g., Jahn et al., 2000) to recycling of originally primitive crustal components (Kröner et al., 2017). Consequently, the underlying mechanism by which the continental crust differentiates still remains rather obscure.

In the present study, we focus on the magmatic evolution of the hornblende-bearing I-type granitoids in the Chinese Altai Orogenic Belt, a high-grade core of the CAOB. These granitoids are medium- to high-K, calc-alkaline, sub-aluminous granitoids (Cai et al., 2011b; Liu et al., 2012; Wang et al., 2006; Yu et al., 2018; Yuan et al., 2007). They were first thought to be derived from arc-related magmatic rocks (e.g., Wang et al., 2006), on account of their apparently subduction-related geochemical characteristics. A petrogenic model of magma mixing between mantle- and crustal-derived magmas was proposed to explain their hybrid crust-mantle geochemistry and variable initial Sr-Nd isotopic compositions (e.g., Wang et al., 2009; Yu et al., 2017a). Their relatively primitive Sr-Nd isotopic signatures have resulted in a tectonic model of large-scale basaltic magma underplating beneath old continental crust (Wang et al., 2009). However, this idea is not supported by recent geochronological studies, which have proven that the previously thought Precambrian continental basement, i.e., high-grade metamorphic rocks, is, in fact, Ordovician wedge sediments (Jiang et al., 2011, 2016; Sun et al., 2008). The so-called “basement rocks” of the Chinese Altai were reinterpreted as variably metamorphosed accretionary wedge complex consisting of an Ordovician sedimentary sequence without any pieces of continental basement (Jiang et al., 2011, 2017; Long et al., 2008; Xiao et al., 2009). In addition, recent structural, metamorphic and geochronological studies indicated that anatexis of Ordovician wedge sediments in the Chinese Altai was coeval with the overwhelming Silurian-Devonian granitoids magmatism in the region (Broussolle et al., 2018; Jiang et al., 2010, 2015, 2019). On the basis of the close temporal and spatial relationship between the anatexis of the Ordovician prism and the Silurian-Devonian peraluminous granitoids as well as their geochemical similarities, Jiang et al. (2016) suggested that the peraluminous granitoids, the majority of Silurian-Devonian granitoids in the region, had originated from partial melting of the wedge sediments. Accordingly, the possibility as to whether the subordinate hornblende-bearing I-type granitoids could have originated from a pre-existing primitive source in the form of basic volcanic admixture or tuffitic layers of the wedge sediments is worth further investigation.

In this study, geological, geochemical and Nd isotopic characteristics of intermediate-to-basic volcanogenic admixtures from the sedimentary rocks of the Ordovician wedge of the Chinese Altai are addressed. In addition, phase equilibrium modelling of melts compositions from melting the volcanogenic components has been performed using the recently available melt model for metabasic rocks of Green et al. (2016). Combined with the results of phase equilibrium modelling, trace element compositions of melts as a function of pressure, temperature and melt fraction were also modelled. Results from this study combined with previously available data, allow us to test the hypothesis that the I-type granitoids in the Chinese Altai had an origin through partial melting of the intermediate-to-basic volcanogenic components of the Ordovician sediments. The results shed light on the differentiation and stabilization of the accretionary wedge in general.

2. Geological setting

The CAOB, also known as the Altaids, extends from the Urals in the west to the Pacific in the east and from the Siberian cratons in the north to the North China and Tarim cratons in the south (Jahn et al., 2000; Şengör et al., 1993; Windley et al., 2007). It is one of the largest and most complex accretionary collages in the world, the formation of which had contributed substantially to the enlargement of the Asian continent by subduction and accretion of juvenile materials from the Neoproterozoic to the late Paleozoic (Şengör et al., 1993; Windley et al., 2007). This giant orogenic system consists of magmatic arcs, ophiolites, accretionary wedges, passive margins, and microcontinents (Şengör et al., 1993; Wilhem et al., 2012). There are controversies surrounding its tectonic evolution, and among which two major competing tectonic models have been proposed, i.e., long-lived subduction and oroclinal bending of a single arc (Şengör et al., 1993; Şengör and Natalin, 1996) versus amalgamation of multiple terranes, similar to the geology of modern SW Pacific (e.g., Windley et al., 2002, 2007; Xiao et al., 2004, 2009, 2010).

The Altai Orogenic Belt is located in the south-central part of the CAOB. It consists mainly of a greenschist- to amphibolite-facies Late Cambro–Ordovician meta-volcano-sedimentary succession (Badarch et al., 2002; Safonova et al., 2009). The whole succession is irregularly covered by Silurian basalt, tuff, and siliciclastic sediments. This thick succession, extending into Mongolia, China, Kazakhstan, and Russia for about 2000 km, was interpreted as a giant accretionary wedge riming the active margin of the northwestern Mongolian Blocks (Jiang et al., 2017; Xiao et al., 2009). It has been suggested that the Cambro-Ordovician geodynamic evolution of the western Mongolian and southern Siberian continental margin was governed by an early compressional and a late extensional event (e.g., Jiang et al., 2017). The first event was responsible for the obduction of Neoproterozoic marginal oceanic basins associated with high-pressure metapelites and eclogites at 540 Ma (Štípská et al., 2010). This occurred almost simultaneously with the emplacement of island arc fragments over the Siberian passive margin (e.g., Glorie et al., 2014; Priyatkina et al., 2016). Turbidite basins located in western Mongolian (e.g., Kuzmichev, 2015) and in the Russian Gorny Altai (e.g., Kruk et al., 2018) were thought to be connected with this event. The second event is attributed to the rollback of the subduction system (Soejono et al., 2016; Jiang et al., 2017), which gave rise to the generation of widespread arc magmatism cumulating at ca. 510 Ma (Janoušek et al., 2018) and high-temperature/low-pressure granulite-facies metamorphism peaking at around 500 Ma (e.g., Gladkochub et al., 2008; Buriánek et al., 2017) in the region. This event may also account for the development of the giant turbidite basin that eventually evolved into a giant accretionary wedge constituting the bulk of the Mongolian and Chinese Altai (Jiang et al., 2017), as investigated in this study. The Chinese segment of the Altai accretionary wedge, namely the Chinese Altai, is characterized by a greywacke-dominated Ordovician metasedimentary sequence and Devonian turbiditic to clastic sedimentary sequences, alternating with NW-SE trending elongated magmatite-migmatite domes (Fig. 1, Broussolle et al., 2019; Xiao et al., 2009). The Chinese Altai is separated from the southerly folded and weakly metamorphosed Silurian-Carboniferous ocean

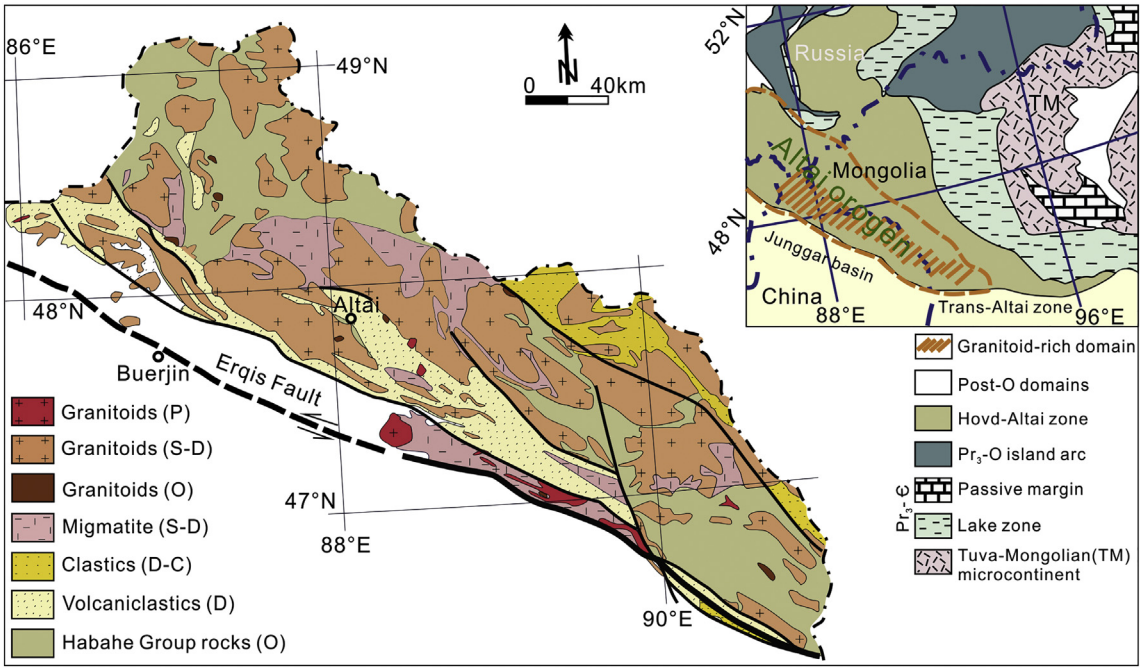

Fig. 1. Geological map of the NW Chinese and western Mongolian tract of the CAOB (upper right) and the geological map of the Chinese Altai (lower left). (After Jiang et al., 2016).

floor sediments and volcanic rocks of the Junggar arc domain by the Erqis fault (Li et al., 2015; Xiao et al., 2009; Zhang et al., 2012). The local geology of the Chinese Altai has been the subject of many studies (e.g., Laurent-Charvet et al., 2003; Li et al., 2017; Wang et al., 2006; Windley et al., 2002; Xiao et al., 2009). Here we summarize available petrological, geochronological and geochemical aspects on the Ordovician sedimentary sequences and Devonian granitoids of the region in the following text.

2.1. Ordovician sedimentary sequence of the Habahe Group

Ordovician sedimentary sequence constitutes the basement of the Chinese Altai, and represents the oldest and most extensive lithological unit, namely the Habahe Group, in the region. It consists of dominant terrigenous-clastic and subordinate volcanoclastic rocks, tuffaceous sediments, and volcanic rocks (Windley et al., 2002; Xiao et al., 2009). The terrigenous sedimentary components are chemically immature and compositionally similar to greywacke (Fig. 2a, see also Jiang et al., 2016; Long et al., 2008). The trace element characteristics of these terrigenous sediments, resemble immature Pacific trench sediments but show lower concentrations of large-ion lithophile elements (LILEs) (e.g., Rb, Sr, Th, U and Pb) and high field strength elements (HFSEs) (e.g., Zr, Hf, Nb, and Ta) than the mature post-Archean Australian shale (PAAS) (Jiang et al., 2016). The terrigenous sedimentary components have active continental margin geochemical affinities (Long et al., 2008). The provenance of the Habahe Group metasedimentary rocks has become the subject of several studies in the past 10 years (e.g., Long et al., 2007, 2008, 2010; Sun et al., 2009; Windley et al., 2002). On the basis of its evolved whole-rock Nd-Sr isotopic compositions as well as Proterozoic Nd model ages (T_{DM}: 1.8–1.5 Ga), Chen and Jahn (2002) suggested that the Habahe Group was composed mostly of evolved continental crustal materials with minor Paleozoic juvenile materials. In contrast, detrital zircons from this sedimentary sequence are characterized by prominent ca. 540–460 Ma grains with subordinate Neoproterozoic and rare pre-Neoproterozoic ones (Broussolle et al., 2019; Jiang et al., 2011; Long et al., 2007). It has also been documented that >70% of the detrital zircons from the Habahe Group have positive zircon $\varepsilon_{Hf}(t)$ values, suggesting that the metasediments contained abundant young and geochemically primitive components (Cai et al., 2011b). It has also been revealed that the main early Paleozoic zircons populations are euhedral and display oscillatory zoning, in contrast to the Precambrian zircons which are generally rounded with complicated magmatic-metamorphic internal structures (Jiang et al., 2011; Long et al., 2007; Sun et al., 2008). Taken together, these features suggest that the detritus for the Habahe Group was mainly derived from both the nearby early Paleozoic arc-proximal sources and perhaps more distant, but certainly more mature, Precambrian continental sources. All these information have led to the interpretation that the Habahe Group rocks probably represent detritus deposited in an active margin setting with significant volcanic input (Jiang et al., 2016; Long et al., 2008). It is noteworthy that an about 1800 km long Cambro-Ordovician Ikh-Mongol arc system was recently defined to the northeast of the Altai Orogenic Belt (Janoušek et al., 2018), and the arc magmatism reworked the accreted Neoproterozoic island arc Lake Zone and Precambrian blocks in western Mongolia (Janoušek et al., 2018). Further comparisons show that the published detrital zircon age patterns of the Habahe Group fit the Neoproterozoic-early Paleozoic arc-related rocks in the Lake Zone and its adjacent Precambrian blocks to the west (Jiang et al., 2011, 2017). This may suggest that the neighboring Lake Zone and its adjacent Precambrian blocks may have significantly contributed to the related Ordovician sedimentary basins in the Chinese Altai. This is also in line with the view that the Habahe Group and its equivalents, stretching from Russia to central Mongolia, represent a huge accretionary wedge riming the active margin of the Precambrian blocks (Jiang et al., 2017; Xiao et al., 2009).

The Altai wedge was transformed into a mature orogenic system during the Devonian Altai orogeny associated with extensive magmatism and synchronous metamorphism (Broussolle et al., 2018; Jiang et al., 2010, 2019; Wang et al., 2006). Petrological observations and thermodynamic modelling suggested that the Habahe Group probably experienced an early Paleozoic Barrovian-

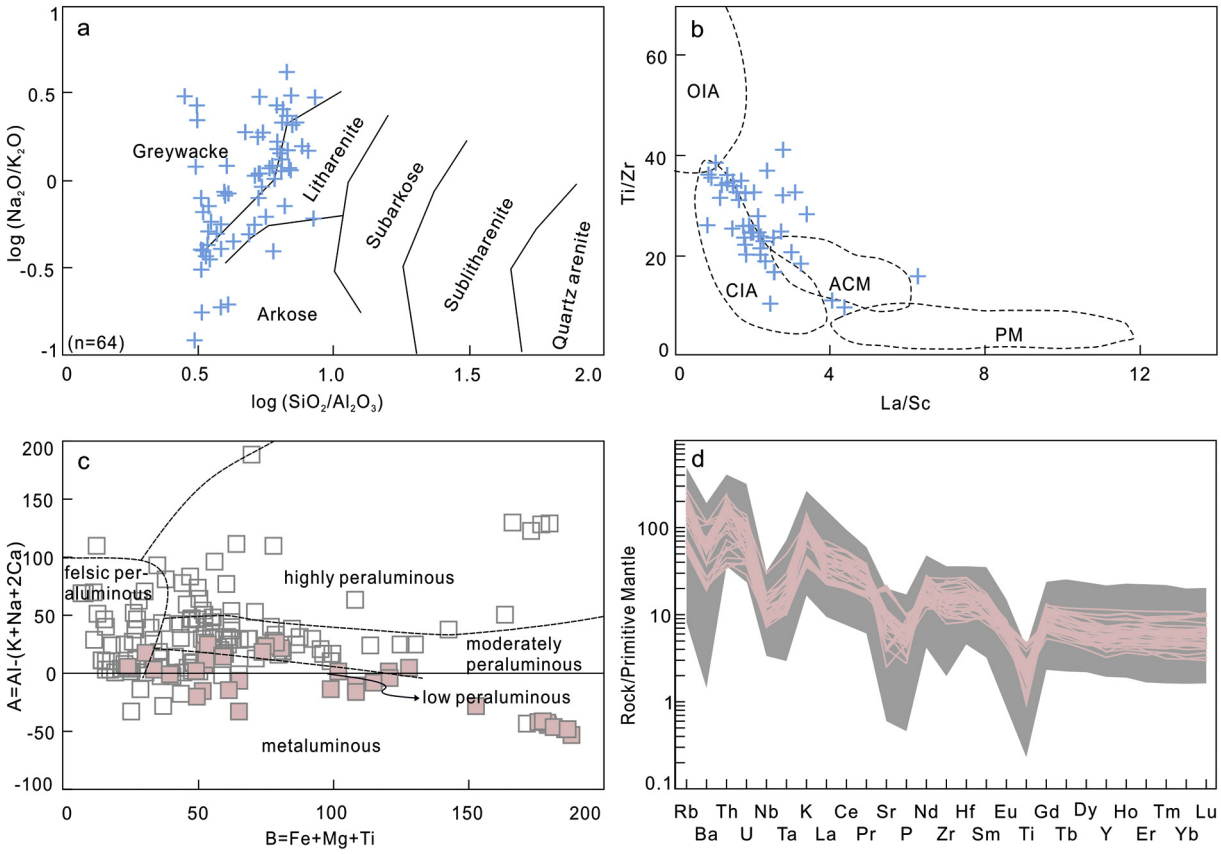

Fig. 2. Geochemical characteristics of the Ordovician Habahe Group terrigenous sedimentary rocks and Silurian-Devonian granitoids from the Chinese Altai. (a) Classification diagram of terrigenous components of the Habahe Group rocks (after Pettijohn et al., 1987), showing their greywacke-dominated nature. (b) La/Sc versus Ti/Zr diagram of the Habahe Group terrigenous components (after Bhatia and Crook, 1986), suggesting a continental arc/active continental margin setting. (c) B-A diagram of Villaseca et al. (1998) modified from Debon (1983) showing that majority of the Silurian-Devonian granitoids from the Chinese Altai are peraluminous compositions (unfilled grey squares), and some "I-type" hornblende-bearing granodiorites and tonalites (filled pink squares) are less peraluminous to metaluminous. (d) Primitive mantle normalized trace element patterns for granitoids (peraluminous granitoids in grey and "I-type" hornblende-bearing granodiorites and tonalites in pink). Primitive mantle normalizing values are from Sun and Mcdonough (1989). Details on data sources are available and presented in Table S1. (For interpretation of the references to color in this figure legend, the reader is referred to the web version of this article.)

Geochemical characteristics of the Ordovician Habahe Group terrigenous sedimentary rocks and Silurian-Devonian granitoids from the Chinese Altai. (a) Classification diagram of terrigenous components of the Habahe Group rocks (after Pettijohn et al., 1987), showing their greywacke-dominated nature. (b) La/Sc versus Ti/Zr diagram of the Habahe Group terrigenous components (after Bhatia and Crook, 1986), suggesting a continental arc/active continental margin setting. (c) B-A diagram of Villaseca et al. (1998) modified from Debon (1983) showing that majority of the Silurian-Devonian granitoids from the Chinese Altai are peraluminous compositions (unfilled grey squares), and some "I-type" hornblende-bearing granodiorites and tonalites (filled pink squares) are less peraluminous to metaluminous. (d) Primitive mantle normalized trace element patterns for granitoids (peraluminous granitoids in grey and "I-type" hornblende-bearing granodiorites and tonalites in pink). Primitive mantle normalizing values are from Sun and Mcdonough (1989). Details on data sources are available and presented in Table S1. (For interpretation of the references to color in this figure legend, the reader is referred to the web version of this article.)

type metamorphism associated with a maximum burial to a depth of 30 km and more (Jiang et al., 2016; Wei et al., 2007). The resulting Barrovian-facies metamorphic rocks were subsequently reworked by regional-scale anatexis at 700–1000 °C with a high field geothermal gradient about 30 °C/km (see also Jiang et al., 2015; Li et al., 2014; Wei et al., 2007). This regional anatexis event was dated at Middle Devonian (390–380 Ma), as revealed by U-Pb dating of metamorphic zircons of migmatitic gneisses (Broussolle et al., 2018; Jiang et al., 2010; Long et al., 2007). These researchers further proposed that the anatexis gave rise to the formation of vertically stratified crust in the Chinese Altai represented by 1) molten or even granulitized Habahe Group forming the orogenic lower crust; 2) greenschist- to amphibolite-facies Habahe Group forming the orogenic middle crust, and 3) low-grade to un-metamorphosed Devonian volcanoclastic succession with surface volcanism representing the orogenic upper crust (see details in Jiang et al., 2019).

2.2. Silurian-Devonian granitoids

Abundant granitoids intruded the Ordovician Habahe sequence and occupy at least 40% of the map surface of the Chinese Altai (Fig. 1, Zou et al., 1989). More than 90% of these granitoids have been emplaced during Late Silurian to Middle Devonian with crystallization U-Pb zircon ages ranging from 420 to 370 Ma and the remaining volumetrically small Late Paleozoic granitoids with emplacement U-Pb zircon ages ranging from 300 to 270 Ma (Tong et al., 2007; Wang et al., 2009). The Silurian-Devonian granitoids form isolated circular or elongate bodies whereas the Late Paleozoic granitoids are spatially concentrated along the southern flank of the Chinese Altai. In the following text, published geological, geochronological and geochemical features of the Silurian-Devonian granitoids are summarized.

Most Silurian-Devonian granitoids were syntectonic, coeval with the formation of the migmatite-magmatite domes. These granitoids are generally surrounded by high-grade gneisses which show progressive textural evolution of migmatite types from

ophthalmitic gneiss, through stromatites to nebulites (Huang et al., 2019; Jiang et al., 2015, 2019). The migmatites are characterized by the mineral assemblage of sillimanite, K-feldspar, garnet and cordierite, attesting to equilibration under granulite-facies conditions (Jiang et al., 2015, 2019; Wei et al., 2007). Relics of Barrovian-series minerals (staurolite and kyanite) were also found in the migmatites (Jiang et al., 2015, 2016), evidencing deep burial of the protolith before the anatectic reworking. Recent U-Pb zircon geochronological studies indicated that emplacement of Silurian-Devonian granitoids culminated at around 400–390 Ma (Cai et al., 2011a), coeval with the high-temperature anatexis of ~390 Ma in the region (Broussolle et al., 2019; Jiang et al., 2010; Long et al., 2007). Abundant early Paleozoic (540–440 Ma) inherited zircons were reported from the granitoids (Cai et al., 2011b; Sun et al., 2008), supporting a widespread Neoproterozoic-Ordovician source component (Jiang et al., 2016). The high proportion of ~500 Ma inherited zircons is comparable with detrital zircon age patterns of the Ordovician Habahe Group metasediments that are characterized by predominantly early Paleozoic ages, peaked at 500 Ma (Broussolle et al., 2019; Jiang et al., 2011, 2017; Sun et al., 2008). This feature obviates the possibility that production of the granitoids from a Proterozoic basement.

Silurian-Devonian granitoids in the region are mainly granodiorites to granites. More than 85% of them are granites to biotite-bearing granodiorites (Bi-granodiorites) and have predominantly peraluminous compositions (Fig. 2c, Jiang et al., 2016). These peraluminous granitoids are characterized by moderate to high SiO_2 contents (65.20–81.60 wt%), moderate total alkalis ($Na_2O + K_2O$, 4.27–8.60 wt%), and high Al_2O_3 contents (10.0–16.7 wt%). The remaining subordinate granitoids are hornblende-bearing granodiorites (Hb-granodiorites) as well as minor tonalites (Fig. S1, Jiang et al., 2016; Liu et al., 2012). They have middle-high SiO_2 (56.80–76.08 wt%), moderate total alkalis (3.65–7.84 wt%), and high Al_2O_3 (11.25–17.10 wt%). The hornblende-bearing granodiorites and tonalites are generally low peraluminous and metaluminous and considered as "I-type" granitoids (e.g., Yu et al., 2017b and reference therein). Despite differences between major element oxides, the peraluminous and "I-type" (metaluminous) granitoids exhibit close trace element chemistry. They have enriched light rare earth elements (LREEs) and flat heavy rare earth elements (HREEs) in chondrite-normalized REE patterns, with moderate to strong negative Eu anomalies (Fig. 2d, see also Jiang et al., 2016). Geologically, the "I-type" granitoids occur always associated with peraluminous granitoids and form peraluminous to metaluminous granitic complexes (e.g., the Hanasi and the Habahe batholiths, see also Wang et al., 2009; Yu et al., 2017b). All of these granitoids show large variations in their zircon $\varepsilon_{Hf}(t)$ values (−7.0 to +9.0), and generally whole-rock negative $\varepsilon_{Nd}(t)$ values (−4.2 to +4.8), which may suggest the addition of juvenile material combined with reworking of old material in the magma source, implying an environment similar to that of an active continental margin, as discussed in many previous studies (Chen and Jahn, 2002; Wang et al., 2009; Yuan et al., 2007; Zhang et al., 2017).

3. Sample descriptions

The dominant phase of the Habahe Group sedimentary succession is a terrigenous clastic sedimentary component, but a subordinate volcanogenic component is also present. This study focuses on the intermediate-to-basic volcanogenic components of the Habahe Group and their roles in the granitoid magmatism in the Chinese Altai. These components occur as either ferromagnesian minerals-enriched admixtures in greenschist-facies rocks or amphibolite layers and/or boudins in amphibolite-facies rocks (Fig. 3a, b). Locally, these volcanic components are preserved as several-meters- to several-hundred-meters-scale massive amphibolites (Fig. 3c). A total of 14 volcanogenic samples were collected for geochemical analysis, 10 of which are interbedded admixture blocks and the other 4 samples are massive amphibolites (see details in Table 1). These samples display more or less similar mineral assemblages, composed mainly of amphibole, biotite, plagioclase and quartz (see Fig. 3d).

4. Analytical methods

Major elements were measured on fused glass disks using a Rigaku ZSX100e X-ray fluorescence spectrometer in the State Key Laboratory of Isotope Geochemistry (SKLIG), Guangzhou Institute of Geochemistry, Chinese Academy of Sciences. Calibration lines used in quantification were produced by bivariant regression of data from 36 reference materials encompassing a wide range of silicate compositions (Li et al., 2005). Analytical precision ranged from 1% to 5%. Trace elements and rare earth elements (REE) were performed using a PerkinElmer Sciex ELAN 6000 ICP–MS in the SKLIG. Powdered samples (~40 mg) were digested using $HNO_3 + HF$ acid mixtures in steel-bomb coated Teflon beakers for two days for complete dissolution of the refractory minerals. The signal drift was monitored by the internal standard solution containing the single element Rh. Sample preparation techniques and other details of procedures are described in Li et al. (2002) and Li et al. (2007). Analytical precision was generally better than 5%. The geochemical data are presented in Table 1.

Nd isotopic analyses were performed on a Micromass Isoprobe multi-collector mass spectrometer (MC-ICP-MS) in SKLIG, following the procedures described by Li et al. (2004a). Measured $^{143}Nd/^{144}Nd$ ratios were normalized to $^{146}Nd/^{144}Nd = 0.7219$. The $^{143}Nd/^{144}Nd$ ratio of the BCR-2 standard measured during this study was 0.512628 ± 15 (2σ). The Nd isotopes results are presented in Table 1.

In order to test the hypothesis that the "I-type" granitoids could have been derived from the Habahe Group volcanogenic components, partial melting equilibrium for the average Habahe intermediate-to-basic volcanogenic components was thermodynamically modelled (Fig. 6a). The thermodynamic modelling was performed using the THERMOCALC 3.45 software package (Powell and Holland, 1988) and the PyPsbuilder front-end (Collett et al., 2018; Lexa, 2017) at P-T conditions of 8–12 kbar, 600–1100 °C (Fig. 6a). Calculations were carried out in the Na_2O-CaO-K_2O-FeO-MgO-Al_2O_3-SiO_2-H_2O-TiO_2-O_2 (NCKFMASHTO) system, using the internally consistent thermodynamic dataset of Holland and Powell (2011, update ds62, 6 February, 2012), and the following a-x models: silicate melt, augite, hornblende (Green et al., 2016); garnet, orthopyroxene, biotite, chlorite, muscovite-paragonite (White et al., 2014); olivine, epidote (Holland and Powell, 2011); magnetite-spinel (White et al., 2002); ilmenite-hematite (White et al., 2000); plagioclase, K-feldspar (Holland and Powell, 2003). A bulk-rock composition was taken from an average composition of 14 intermediate-to-basic volcanogenic samples (Table 1). This composition was then corrected for the presence of unmodelled elements (e.g., all P_2O_5 is assumed to be bound in apatite and is extracted along with an equivalent amount of CaO). As only ilmenite is observed in the samples and because unaltered basic igneous rocks typically show low oxidation state (Schilling et al., 1983), the bulk rock $X^{3+}_{Fe} = Fe^{3+}/(Fe^{2+} + Fe^{3+})$ ratios were fixed at a low value (0.12, see Rebay et al., 2010). The amount of H_2O was set to allow for minimally saturated melting at 10 kbar, which allows for the modelling of the partial melting process in a H_2O-closed system. Following the procedure in Jiang et al. (2016) representative compositions of melts (normalized to 100% on an anhydrous basis) were investigated at 8, 10 and 11.5 kbar. The compositions of modelled melts are presented in Table 2 and plotted in Fig. 6.

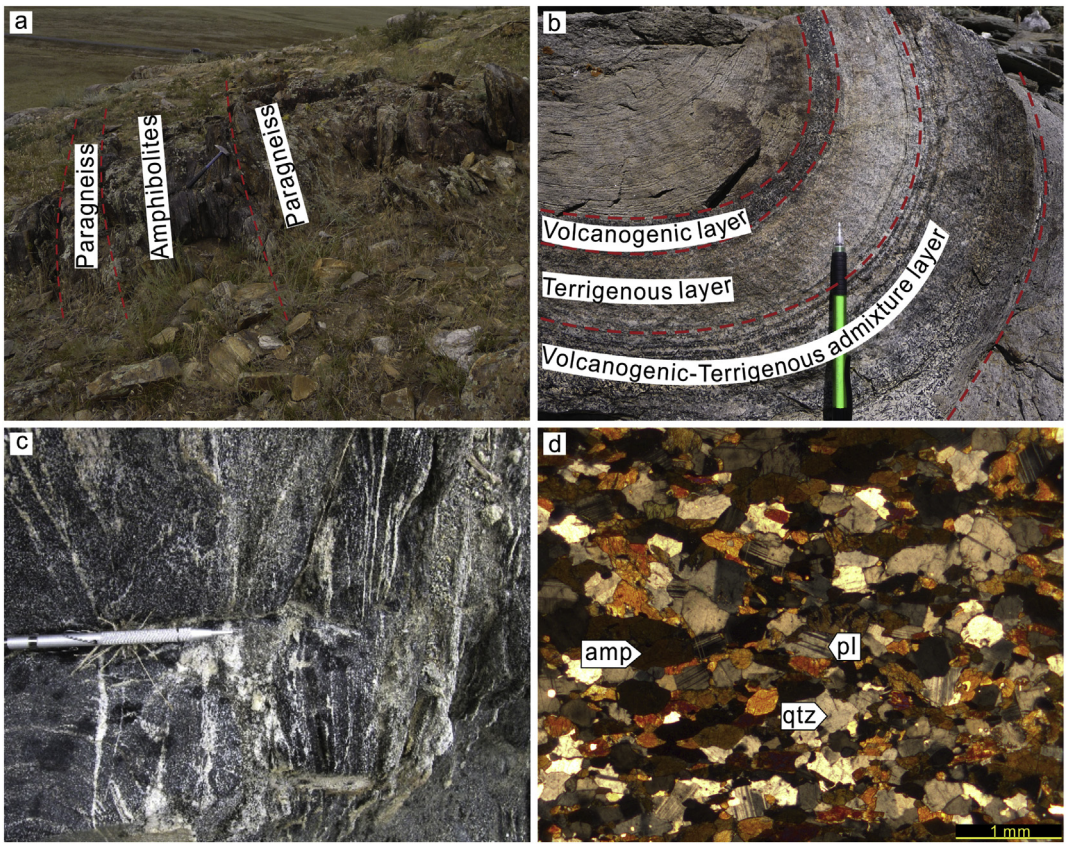

Fig. 3. (a) Amphibolite boudins preserved in the metamorphosed Habahe Group succession. (b) Intermediate-to-basic layer (dark horizons, upper) and admixture (lower) interlayered with terrigenous components of the Habahe Group. (c) Partially molten massive amphibolite of the Habahe Group. (d) Photomicrographs of amphibolite within the Habahe Group. Mineral abbreviations are amp-amphibole, pl-plagioclase, qtz-quartz.

The above phase equilibrium modelling could allow calculation of the abundance and composition of partial melt and residual minerals. Representative melts that are compositionally comparable with the investigated I-type granitoids are selected for further trace element modelling. For such modelling, the abundance and composition of residual minerals were computed directly via THERMOCALC software, and published mineral/melt partition coefficients from previous studies were applied (Table S4). The calculated processes and results are presented in Table S4 and Fig. 7.

5. Results

5.1. Major and trace elements

Geochemical compositions of intermediate-to-basic volcanogenic samples are presented in Table 1. These samples have compositions varied from basalt to basaltic andesite in terms of their SiO_2 concentrations (46.30–52.56 wt%, Fig. 4a). They have relatively high MgO (5.32–8.18 wt%) and $Na_2O + K_2O$ (3.13–5.35 wt%) contents, low K_2O/Na_2O (0.03–0.54 wt%) ratios, and middle-to-high FeO^T (7.18–13.73 wt%), TiO_2 (1.17–2.84 wt%) and Al_2O_3 (13.69–17.15 wt%) contents. These features make them mostly falling into the calc-alkaline field in the FeO^T-$Na_2O + K_2O$-SiO_2 discrimination diagram (Fig. 4b). They display sub-parallel REE patterns with enrichment in LREE ($La_N/Yb_N = 2.06–6.99$), flat HREE ($Gd_N/Yb_N = 1.66–2.09$) and weak negative Eu anomalies (Fig. 4c). On a primitive mantle (PM)-normalized variation diagram, most samples show enrichment in LILEs (e.g., Rb, Sr, Th and U) and pronounced negative Nb, Ta, and Ti anomalies (Fig. 4d), compatible with a subduction-related environment. Broadly, the massive amphibolite samples have relatively lower SiO_2 and higher FeO^T contents compared to those of volcanogenic admixture samples. The relatively less differentiated REE patterns and higher Ti/Zr and Co/Th ratios of the former imply that they are probably derived from less evolved mantle source (Fig. 4e, f).

5.2. Nd isotopic composition

The Nd isotopic data of 14 volcanogenic samples are presented in Table 1 and plotted in Fig. 5, alongside with 8 previously published data. For further comparison, Nd isotopic data of the 59 Silurian-Devonian granitoids and 31 Habahe terrigenous samples of the Chinese Altai are also plotted (data in Table S2). The $\varepsilon_{Nd}(400\ Ma)$ values of the analyzed samples vary from +4.1 to +9.1, similar to or slightly more positive than the previously published data of volcanogenic samples (Fig. 5a). It is notable that the massive amphibolite samples are more radiogenic than the volcanogenic admixture samples, advocating the notion that the amphibolite samples are chemically more primitive as cited above (Fig. 5a). The Nd isotopic signatures of the bulk volcanogenic samples are generally more radiogenic than most local granitoids. The two-stage depleted mantle Nd model ages of the investigated volcanogenic samples are 0.4–0.9 Ga, younger than those of most granitoids (0.6–1.5 Ga, Wang et al., 2009). This is consistent with the widely accepted view that the Habahe Group contains abundant geochemically primitive components (Cai et al., 2011a; Jiang et al., 2016; Liu et al., 2012; Long et al., 2012). It is noteworthy that the $\varepsilon_{Nd}(400\ Ma)$ values of bulk Habahe terrigenous components vary from −6.1 to +2.6 (mostly negative, see also Jiang et al., 2016), a range somewhat less radiogenic than most local granitoids

Table 1
Major (wt%) and trace (ppm) element and Nd isotopic compositions of volcanogenic components of the Habahe Group in the Chinese Altai.

Sample	BC01	BC02	BC03	BC04	BC05	BC06	CA01	CA02	CA03	CA04	ALT01	ALT02	ALT03	ALT04
Location	48°2′52.30″N, 86°58′5.40″E						47°49′27.99″N, 88°1′25.79″E				47°48′46.98″N, 88°2′47.64″E			
SiO_2	52.15	52.56	51.88	51.63	51.69	52.00	46.67	46.30	46.75	47.08	50.97	51.05	51.58	48.94
TiO_2	1.25	1.22	1.20	1.17	1.26	1.26	2.83	2.78	2.84	2.54	1.16	1.37	1.36	2.05
Al_2O_3	17.01	16.90	16.93	16.94	16.76	17.15	13.74	13.69	13.86	14.02	16.17	16.26	16.22	16.08
FeO^T	7.18	7.86	8.46	8.04	8.29	8.36	13.73	13.62	13.64	13.01	7.36	8.00	8.06	9.65
MnO	0.13	0.14	0.15	0.14	0.15	0.14	0.26	0.27	0.27	0.27	0.16	0.17	0.16	0.17
MgO	5.32	6.10	6.21	5.60	6.14	6.00	6.68	6.61	6.56	6.77	7.61	7.29	8.18	7.33
CaO	9.61	8.32	8.19	8.73	8.40	8.71	11.20	11.10	11.10	11.10	8.10	7.03	7.70	7.85
Na_2O	4.14	4.79	4.85	4.43	4.65	4.68	2.59	2.53	2.61	2.63	3.18	3.68	2.97	3.16
K_2O	0.20	0.17	0.18	0.16	0.19	0.16	0.61	0.60	0.60	0.63	1.71	1.67	0.74	1.43
P_2O_5	0.31	0.28	0.31	0.29	0.31	0.32	0.33	0.33	0.34	0.27	0.24	0.28	0.27	0.27
LOI	0.83	0.90	0.83	1.01	0.91	0.82	0.40	0.55	0.44	0.52	1.78	2.05	1.60	2.17
Total	98.13	99.24	99.19	98.14	98.75	99.60	99.04	98.38	99.01	98.84	98.44	98.85	98.84	99.10
Mg#	60.84	61.93	60.62	59.35	60.84	60.08	50.50	50.43	50.21	52.18	68.44	65.65	68.03	61.42
$Na_2O + K_2O$	4.34	4.96	5.03	4.59	4.84	4.84	3.20	3.13	3.21	3.26	4.89	5.35	3.71	4.59
Sc	32.3	34.4	34.0	30.6	33.9	32.8	44.6	46.5	46.2	45.5	28.7	23.7	26.1	27.7
V	264	257	267	239	258	267	475	493	483	480	171	169	165	233
Cr	120	120	130	120	130	130	180	190	180	190	340	270	310	230
Co	17.8	24.0	27.2	23.8	26.8	27.1	41.5	45.4	45.6	42.6	34.3	36.9	37.3	42.6
Ni	30.4	34.2	36.0	30.3	34.6	33.6	51.0	53.8	53.7	54.5	134.0	132.0	134.5	128.5
Ga	19.95	19.70	18.85	19.20	18.65	18.80	21.1	21.9	21.5	21.0	16.60	16.65	17.20	17.65
Cs	0.24	0.16	0.12	0.13	0.15	0.07	0.05	0.02	0.03	0.09	0.86	0.69	0.71	0.76
Rb	5.4	3.1	2.7	2.6	2.8	1.8	6.6	6.5	6.5	9.5	88.9	99.1	31.1	80.5
Ba	13.6	29.8	14.9	13.7	12.5	8.7	30.3	28.4	30.2	30.2	150.0	149.5	117.0	163.5
Th	2.15	1.96	1.94	1.91	2.08	2.00	0.30	0.38	0.32	0.46	1.97	2.47	2.50	2.14
U	0.61	0.67	0.78	0.72	0.76	0.78	0.46	0.38	0.38	0.44	0.84	0.91	0.89	0.73
Pb	3.7	4.4	3.7	4.0	3.7	3.5	3.0	2.4	2.2	2.9	10.3	12.6	7.6	8.4
Nb	5.3	5.2	5.1	5.3	5.2	5.2	7.8	8.1	8.0	6.6	6.4	7.8	7.5	8.3
Ta	0.43	0.24	0.25	0.46	0.36	0.36	0.49	0.50	0.51	0.40	0.20	0.47	0.45	0.49
Sr	710	400	381	518	405	444	220	230	238	222	428	359	462	475
Y	30.3	29.2	29.1	28.7	29.3	29.7	50.8	51.3	51.7	44.3	23.2	24.4	23.5	26.5
Zr	153	136	141	143	146	152	230	228	239	184	147	166	162	151
Hf	3.5	3.3	3.6	3.4	3.7	3.4	5.4	5.6	5.5	4.3	3.3	3.7	3.5	3.3
La	17.5	15.9	16.8	14.8	15.6	15.7	10.1	10.5	10.3	9.3	12.8	15.8	14.7	15.3
Ce	41.6	39.0	41.9	36.4	39.6	38.7	28.2	29.2	29.0	24.6	29.5	35.5	33.6	34.5
Pr	5.54	5.20	5.46	5.12	5.22	5.15	4.50	4.72	4.62	3.93	3.96	4.71	4.52	4.65
Nd	24.1	23.7	23.9	22.8	23.4	22.9	22.7	23.9	23.4	19.8	17.2	20.1	19.1	20.1
Sm	5.59	5.36	5.33	5.15	5.33	5.24	6.69	7.02	6.87	5.81	4.02	4.40	4.30	4.71
Eu	1.80	1.63	1.63	1.57	1.60	1.59	2.23	2.26	2.23	1.96	1.33	1.41	1.40	1.49
Gd	5.48	5.43	5.18	5.12	5.25	5.25	8.14	8.51	8.29	7.12	4.04	4.55	4.47	4.98
Tb	0.87	0.85	0.82	0.80	0.83	0.83	1.39	1.44	1.43	1.22	0.64	0.72	0.72	0.81
Dy	5.22	5.11	5.04	4.91	5.06	4.90	8.87	9.27	9.01	7.76	4.05	4.46	4.32	4.84
Ho	1.11	1.07	1.05	1.01	1.08	1.04	1.90	1.98	1.94	1.68	0.84	0.91	0.88	1.00
Er	3.06	2.98	2.97	2.89	3.00	2.92	5.37	5.60	5.50	4.76	2.31	2.54	2.53	2.74
Tm	0.45	0.44	0.42	0.41	0.42	0.43	0.79	0.81	0.79	0.68	0.33	0.36	0.37	0.39
Yb	2.83	2.67	2.64	2.57	2.64	2.63	4.90	5.00	4.94	4.25	2.09	2.26	2.24	2.38
Lu	0.41	0.40	0.40	0.38	0.40	0.40	0.74	0.76	0.73	0.63	0.32	0.35	0.34	0.36

(*continued on next page*)

Table 1 (*continued*)

Sample	BC01	BC02	BC03	BC04	BC05	BC06	CA01	CA02	CA03	CA04	ALT01	ALT02	ALT03	ALT04
Location	48°2′52.30″N, 86°58′5.40″E						47°49′27.99″N, 88°1′25.79″E				47°48′46.98″N, 88°2′47.64″E			
$^{143}Nd/^{144}Nd$[e]	0.512713	0.512727	0.512723	0.512726	0.512724	0.512740	0.513057	0.513050	0.513046	0.513054	0.512810	0.512757	0.512734	0.512768
2σ	0.000007	0.000009	0.000008	0.000011	0.000008	0.000008	0.000007	0.000008	0.000008	0.000009	0.000007	0.000010	0.000010	0.000009
$^{147}Sm/^{144}Nd$[a]	0.1404	0.1369	0.1350	0.1365	0.1379	0.1383	0.1781	0.1778	0.1778	0.1777	0.1412	0.1323	0.1364	0.1416
$(^{143}Nd/^{144}Nd)_t$	0.512345	0.512368	0.512369	0.512369	0.512363	0.512378	0.512591	0.512584	0.512580	0.512588	0.512440	0.512411	0.512377	0.512397
$\varepsilon_{Nd}(t)$[b]	4.3	4.8	4.8	4.8	4.7	5.0	9.1	9.0	8.9	9.1	6.2	5.6	5.0	5.4
$T_{DM}(Ga)$[c]	0.9	0.8	0.8	0.8	0.9	0.8	0.4	0.4	0.4	0.4	0.7	0.7	0.8	0.8
$T_{2DM}(Ga)$[f]	0.8	0.8	0.8	0.8	0.8	0.7	0.4	0.4	0.4	0.4	0.6	0.7	0.7	0.7
$f_{Sm/Nd}$[d]	−0.29	−0.30	−0.31	−0.31	−0.30	−0.30	−0.09	−0.10	−0.10	−0.10	−0.28	−0.33	−0.31	−0.28
						0.30								

[a] $^{147}Sm/^{144}Nd$ are calculated using whole-rock Sm and Nd contents.

[b] $\varepsilon_{Nd}(t) = [(^{143}Nd/^{144}Nd)_S/(^{143}Nd/^{144}Nd)_{CHUR} - 1] \times 10{,}000$.

[c] $T_{DM} = 1/\lambda_{sm} \times \ln[1 + ((^{143}Nd/^{144}Nd)_S - 0.51315)/((^{147}Sm/^{144}Nd)_S - 0.2137)] \times 1000$.

[d] $f_{Sm/Nd} = [(^{147}Sm/^{144}Nd)_S/(^{147}Sm/^{144}Nd)_{CHUR}] - 1$.

[e] In the calculation, $(^{143}Nd/^{144}Nd)_{CHUR} = 0.512638$; $(^{147}Sm/^{144}Nd)_{CHUR} = 0.1967$; $\lambda_{sm} = 6.54 \times 10^{-6}$ where S, CHUR are the sample and Chondritic Uniform Reservoir.

[f] t is using the age of 400 Ma, because the present study wants to compare the initial $^{143}Nd/^{144}Nd$ ratios, $\varepsilon_{Nd}(t)$ values and model ages of the Habahe rocks with those of magmatic rocks in the region, which have predominant ca. 400 Ma emplacement ages.

Table 2
Compositions of modelled melts from partial melting of the Habahe Group volcanogenic components (normalized to 100 wt% anhydrous).

Melt	P-T (kbar/°C)	Residue assemblage	SiO_2	Al_2O_3	FeO	MgO	CaO	Na_2O	K_2O
1	8/650	Cam Pl Cpx Bt Ttn Qtz	73.99	15.39	0.03	0.01	1.41	5.50	3.68
2	8/700	Cam Pl Cpx Bt Ttn Qtz	73.95	15.33	0.09	0.03	1.55	5.29	3.75
3	8/750	Cam Pl Cpx Bt Ttn Qtz	73.74	15.27	0.29	0.09	1.73	4.99	3.89
4	8/800	Cam Pl Cpx Bt Rt Qtz	73.09	15.21	0.79	0.23	2.03	4.38	4.27
5	8/850	Cam Pl Cpx Opx Rt	71.94	15.24	1.64	0.51	2.34	4.07	4.24
6	8/900	Cam Pl Cpx Opx Rt	68.07	16.31	3.26	1.17	2.50	5.18	3.50
7	8/950	Cam Pl Cpx Opx Rt	64.52	16.63	5.36	2.23	2.73	5.76	2.77
8	8/1000	Cam Pl Cpx Opx Rt	61.75	16.67	6.91	3.49	3.06	5.97	2.15
9	8/1050	Cam Pl Cpx Opx Rt	59.82	16.87	7.36	4.73	3.55	5.95	1.71
10	8/1100	Pl Cpx Opx Rt	58.75	17.24	7.05	5.56	4.28	5.69	1.42
11	10/650	Cam Pl Cpx Bt Ttn Qtz	72.67	16.11	0.02	0.01	1.52	5.27	4.41
12	10/700	Cam Pl Cpx Bt Ttn Qtz	72.77	16.03	0.07	0.02	1.66	5.15	4.30
13	10/750	Cam Pl Cpx Bt Ttn Qtz	72.72	15.94	0.21	0.06	1.84	4.88	4.34
14	10/800	Cam Pl Cpx Bt Rt Qtz	72.31	15.84	0.58	0.16	2.18	4.19	4.74
15	10/850	Cam Pl Cpx Rt Qtz	71.40	15.72	1.45	0.40	2.46	3.74	4.83
16	10/900	Cam Pl Cpx Opx Rt	69.62	16.12	2.60	0.82	2.74	4.46	3.65
17	10/950	Cam Pl Cpx Opx Rt	65.81	16.78	4.60	1.66	2.93	5.27	2.95
18	10/1000	Cam Pl Cpx Opx Rt	62.60	16.96	6.45	2.80	3.20	5.67	2.31
19	10/1050	Cam Pl Cpx Opx Rt	60.36	17.17	7.25	3.98	3.61	5.80	1.83
20	10/1100	Cam Pl Cpx Opx Rt	58.74	17.61	7.14	5.08	4.22	5.72	1.48
21	11.5/700	Cam Pl Cpx Bt Ttn Qtz	71.84	16.50	0.05	0.02	1.79	4.71	5.10
22	11.5/750	Cam Pl Cpx Bt Ttn Qtz	71.91	16.40	0.16	0.05	1.97	4.52	4.99
23	11.5/800	Cam Pl Cpx Bt Rt Qtz	71.58	16.32	0.45	0.12	2.34	3.80	5.39
24	11.5/850	Cam Pl Cpx Rt Qtz	71.01	16.20	1.17	0.31	2.61	3.61	5.10
25	11.5/900	Cam Pl Cpx Opx Rt Qtz	69.84	16.10	2.53	0.70	2.85	3.92	4.06
26	11.5/950	Cam Pl Cpx Opx Rt	66.81	16.83	4.04	1.32	3.12	4.81	3.07
27	11.5/1000	Cam Pl Cpx Opx Rt	63.32	17.17	6.03	2.34	3.35	5.37	2.42
28	11.5/1050	Cam Pl Cpx Opx Rt	60.79	17.41	7.10	3.47	3.70	5.62	1.91
29	11.5/1100	Cam Pl Cpx Opx Rt	59.05	17.84	7.14	4.54	4.24	5.65	1.54

(Fig. 5a). In the same way, the Nd model ages (T_{2DM}) of the bulk granitoids in the Chinese Altai vary broadly between 1.0 and 1.4 Ga, falling in the gap between those ages of the Habahe Group terrigenous and volcanogenic components (Fig. 5b, see also Huang et al., 2019). Clearly, the Nd isotopic signatures of nearly all granitoids can be attained by mixing in the source of the terrigenous and volcanogenic components in various proportions. It is therefore possible to envisage that the Habehe Group metasediments could potentially be the source of the local granitoids, including the hornblende I-type granitoids.

5.3. Thermodynamic modelling

Within the modelled P-T range (6–12 kbar and 600–1100 °C) the onset of partial melting is predicted to occur at between 620 and 680 °C (Fig. 6a). At the H_2O-saturated solidus, the predicted assemblage consists of hornblende, clinopyroxene, plagioclase, biotite, quartz, and titanite at lower pressures. Epidote and muscovite are additionally stable above 9 kbar and above 11 kbar, respectively. Biotite dehydration takes place between 815 and 840 °C, while hornblende is progressively destabilized with increasing temperature and eventually disappears above 1050 °C. Growth of orthopyroxene associated with destabilization of quartz, occurs at 810 °C at 6 kbar increasing to 920 °C at 12 kbar. Broadly, only a small amount of melt (<10 vol%) is generated prior to the biotite dehydration reaction, however, melt production increases significantly associated with destabilization of hornblende, which could generate >50 vol% of melts by the hornblende dehydration reaction at >1050 °C.

Compositions of 29 representative modelled melts are further studied. The detailed composition of these melts can be seen in Table 2 and Fig. 6. The initial melt produced at the solidus is enriched in SiO_2, Na_2O, and K_2O and poor in both FeO and MgO (Fig. 6b). In general, the melt is slightly SiO_2-poorer and the K_2O/Na_2O ratios increase significantly with increasing pressure. On the other hand, SiO_2 contents of the melts decrease slowly in the presence of quartz before decreasing rapidly beyond the quartz stability field, from low to high temperature conditions. FeO, MgO and, to a lesser extent, CaO contents all increase with increasing temperature and the X_{Fe} decreases from initially around 75% at 650 °C to 56–61% at 1100 °C. The K_2O/Na_2O ratio initially increases with increasing temperature before decreasing rapidly after the biotite dehydration reaction. Therefore, it can be concluded that the major element compositions of the resultant melts mainly depend on temperature. Predicted is progressive destabilization of biotite, quartz and hornblende, contemporaneous with systematic decrease of SiO_2 and K_2O and increase of CaO, MgO and FeO contents in the melts with increasing temperature (Figs. 6, S2, S3 and S4). In general, the modelled melts evolved from granite, via granodiorite, to tonalite compositions, with increasing temperature. Melts at lower temperatures (<850 °C) are compositionally similar to those modelled from partial melting of terrigenous components of the Habahe Group, both of which are overlapping with most local granites to biotite-granodiorites of the Chinese Altai (Fig. 6c, d). In contrast, melts at higher temperatures, which are in equilibrium with hornblende-orthopyroxene-bearing assemblage, have granodioritic to tonalitic compositions, which are comparable to those of experimental melts derived from quartz amphibolites (Fig. 6c, d, Patiño Douce and Beard, 1995). In general, these modelled melts broadly cover the whole range of the hornblende-granodiorites and tonalites in the region (Fig. 6c, d).

As pointed out by Jiang et al. (2016), the modelled melts compositions provide only constraints on the nature of the liquids. However, most granitoids are rather complex solid-liquid suspensions than simple partial melts. In addition, it is most likely that partial melts would undergo a variety of physical and chemical processes and interactions, including assimilation, fractional crystallization, and crystal accumulation from their source region on the way to the surface. Besides, partial melts generated from volcanogenic components would virtually mix with those from terrigenous components in some stage, which might generate vast complexity of melt composition. These may alternatively explain

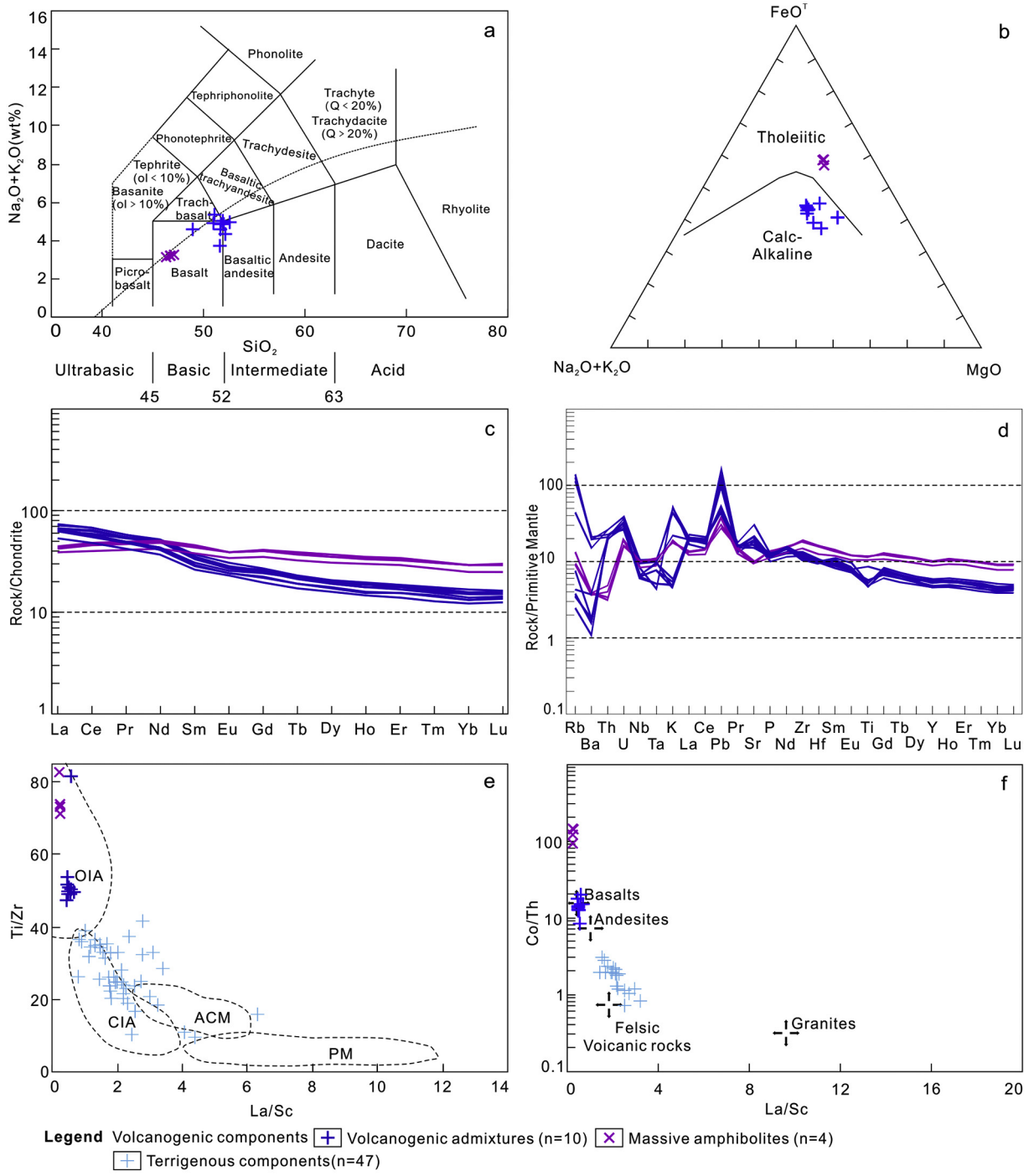

Fig. 4. Geochemical characteristic of intermediate-to-basic volcanogenic components of the Habahe Group in the Chinese Altai. (a) TAS diagram of volcanogenic components shows compositions varied from basalt to basaltic andesite (after Le Maitre et al., 1989). (b) FeO^T-$Na_2O + K_2O$-MgO diagram shows calc-alkaline affinities (after Irvine and Baragar, 1971). (c) Chondrite-normalized REE pattern and (d) PM-normalized spider diagram of volcanogenic components. Chondrite and Primitive mantle normalizing values are from Sun and Mcdonough (1989). (e) La/Sc versus Ti/Zr diagram of volcanogenic components (after Bhatia and Crook, 1986), suggesting compositionally comparable with oceanic island arc rocks. Data of Habahe terrigenous components is also shown for comparison. Outlined fields: OIA = oceanic island arc; CIA = continental arc; ACM = active continental margin; and PM = passive margin. (f) La/Sc versus Co/Th diagram (after McLennan et al., 1984; Condie et al., 1992; Gu et al., 2002), showing derivation mainly from mixed intermediate-basic volcanic source. Related data are presented in Tables 1 and S1.

Geochemical characteristic of intermediate-to-basic volcanogenic components of the Habahe Group in the Chinese Altai. (a) TAS diagram of volcanogenic components shows compositions varied from basalt to basaltic andesite (after Le Maitre et al., 1989). (b) FeO^T-$Na_2O + K_2O$-MgO diagram shows calc-alkaline affinities (after Irvine and Baragar, 1971). (c) Chondrite-normalized REE pattern and (d) PM-normalized spider diagram of volcanogenic components. Chondrite and Primitive mantle normalizing values are from Sun and Mcdonough (1989). (e) La/Sc versus Ti/Zr diagram of volcanogenic components (after Bhatia and Crook, 1986), suggesting compositionally comparable with oceanic island arc rocks. Data of Habahe terrigenous components is also shown for comparison. Outlined fields: OIA = oceanic island arc; CIA = continental arc; ACM = active continental margin; and PM = passive margin. (f) La/Sc versus Co/Th diagram (after McLennan et al., 1984; Condie et al., 1992; Gu et al., 2002), showing derivation mainly from mixed intermediate-basic volcanic source. Related data are presented in Tables 1 and S1.

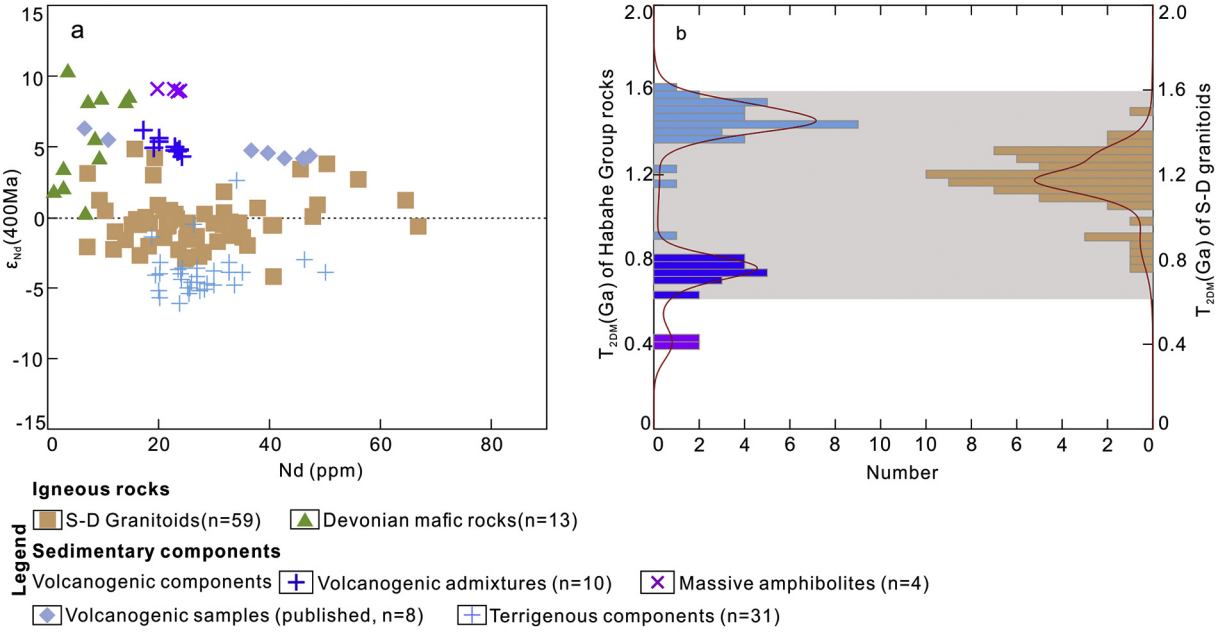

Fig. 5. (a) Diagram of ε_{Nd}(400 Ma) versus Nd (ppm) for sedimentary rocks of the Habahe Group rocks, and Silurian-Devonian igneous rocks; (b) two stage Nd model ages of the Habahe Group rocks and the granitoids. Details are available in Tables 1 and S2.
(a) Diagram of ε_{Nd}(400 Ma) versus Nd (ppm) for sedimentary rocks of the Habahe Group rocks, and Silurian-Devonian igneous rocks; (b) two stage Nd model ages of the Habahe Group rocks and the granitoids. Details are available in Tables 1 and S2.

larger variation in chemistry of the granitoids compared to the compositions of modelled partial melts (Fig. 6c, d).

5.4. Trace element modelling

As shown above that melts modelled at 900–1000 °C, irrespective of pressure, with melt fractions ranging from 15 to 35 vol%, are compositionally matched with the investigated hornblende-bearing I-type granitoids. Using the calculated abundance of residual minerals formed in equilibrium with melts at different temperatures (i.e., different melt fractions, Table S4), and appropriate mineral/melt partition coefficients, we further model the trace element composition of melts that are in equilibrium with amphibolite + two-pyroxene + rutile + plagioclase at the P-T range of 8–11.5 kbar and 900–1000 °C (see Table S4). Despite the differences in abundance of residual minerals and melt fractions, it is shown that almost all melts have very similar trace element composition (Fig. 7). They are characterized by fractionated REE patterns with weakly negative Eu anomalies (Fig. 7a). On the primitive mantle normalized diagram, these melts are significantly depleted in Nb, Ta, Sr and Ti and enriched in LILE, such as Th and U (Fig. 7b). More importantly, the modelled melts show excellent match, in terms of REE abundances and distribution patterns, with the hornblende-granodiorites and tonalites in the Chinese Altai (Fig. 7b). It should be noted that the calculated HREE concentrations are slightly higher than those of hornblende-bearing granitoids in the region (Fig. 7). This may due to that the accessory minerals, such as zircon and apatite, which were not considered in the trace elemental modelling, since these accessory phases could not be modelled during the phase equilibrium modelling as shown in Fig. 6a.

6. Discussion

6.1. A new perspective on magma source of the Altai granitoids

The Silurian-Devonian granitoids in the Chinese Altai were classically interpreted as a product of arc magmatism, on the basis of their arc-like geochemical characteristics (Cai et al., 2010; Wang et al., 2006; Yuan et al., 2007). The related magmatic arc was thought to be a continental-type arc since an old Precambrian basement was believed to exist in the region (e.g., Tong et al., 2007; Wang et al., 2006). However, this idea is not compatible with recent findings which have proven that Precambrian continental basement does not exist (e.g., Jiang et al., 2011; Sun et al., 2008). It is therefore highly speculative regarding the proposed whole petrogenetic model of the granitoids. In contrast, Jiang et al. (2016) illustrated that the Devonian partial melting of fertile Ordovician terrigenous metasediments of the Habahe Group could be sufficient enough to produce large volumes of granitic to granodioritic melts, compositionally resembling most local granitoids. Hence, those authors reinterpreted that, at least, the predominant (~85 vol%) peraluminous granitoids (granites to biotite-granodiorites) could have originated by anatexis of the Habahe metasedimentary rocks. The question of as whether the remaining subordinate relatively Ca-Mg rich hornblende-bearing "I-type" granodiorites to tonalites could have also derived from partial melting of the Habahe Group rocks thus calls for further investigation.

Partial melting of the intermediate-to-basic volcanogenic components in the Habahe Group could probably provide a viable source for these hornblende-granodiorites to tonalites. Previous petrological observations and metamorphic modelling suggested that the crustal anatexis reworking of the Habahe Group at deep orogenic crustal levels (30–40 km) could attain temperature close to almost 1000 °C (e.g., Broussolle et al., 2018; Jiang et al., 2016; Wei et al., 2007 and references therein). Phase equilibrium modelling in this work shows that partial melting of the volcanogenic components could produce a large amount of melt at attainable pressure-temperature conditions (Fig. 6a). Progressive decomposition of biotite, quartz and hornblende has resulted in the generated melts evolving from granitic to granodioritic compositions (Fig. 6b, c and d), the latter is comparable with most hornblende-granodiorites to tonalites in the region (Fig. 6c, d).

Trace element geochemical characteristics of the investigated samples displayed apparent arc-related geochemical affinities, including fractionated REE patterns, enrichment in LILE, and

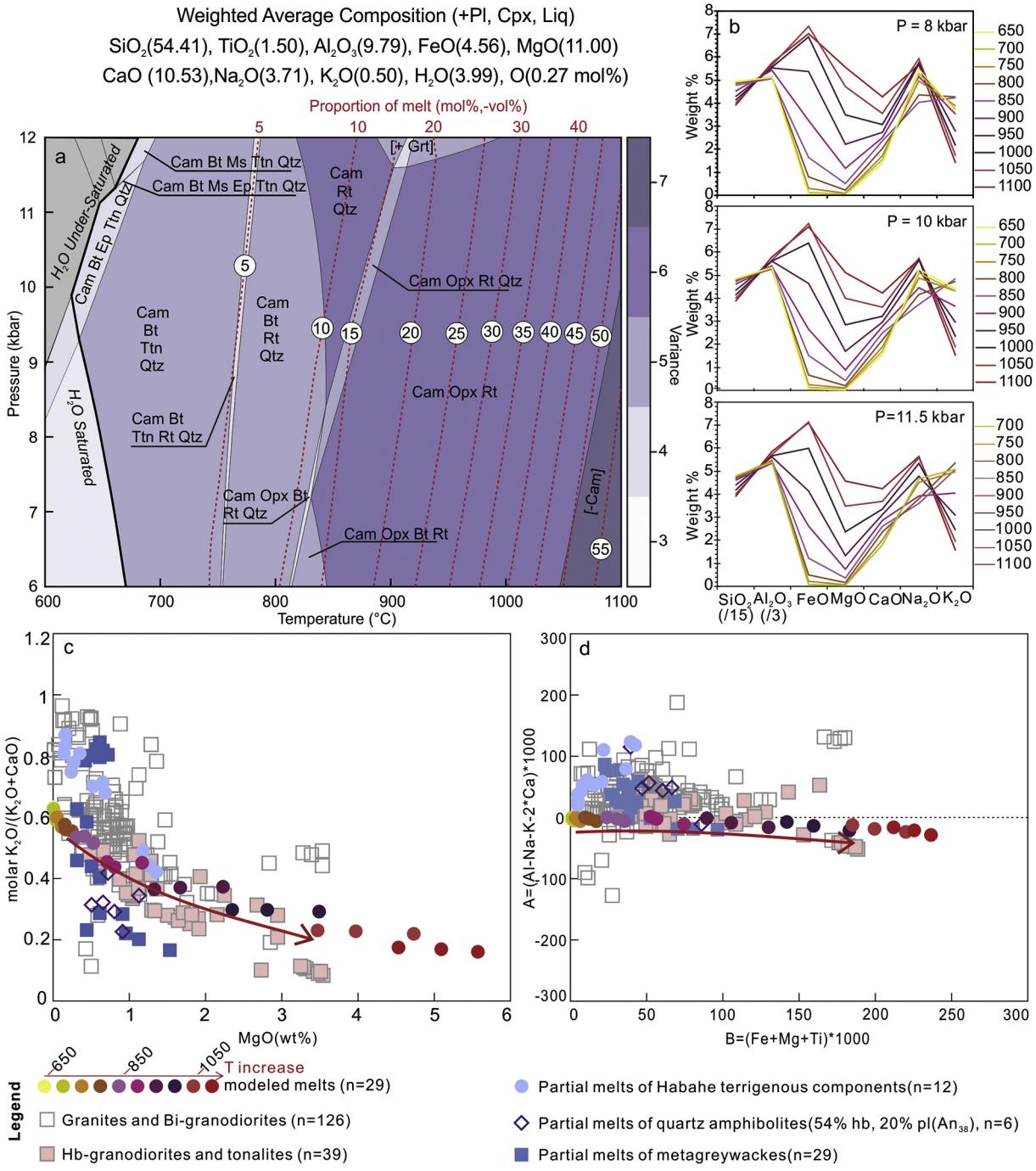

Fig. 6. (a) P-T pseudosection for the average Habahe Group volcanogenic components with calculated melt proportion isopleths. P-T conditions and compositions of the modelled melts are presented in Table 2. (b) Contents of representative oxides plotted versus pressure and temperature (see also Figs. S2, S3 and S4). (c) Whole-rock chemical projection for modelled melts from this study, partial melts modelled from terrigenous components of Jiang et al. (2016) and granitoids of the Chinese Altai are shown for comparison. (d) Multicationic A-B diagram after (Castro et al., 2010). Compositions of partial melts from melting experiments of quartz amphibolites (Patiño Douce and Beard, 1995), and metagreywackes (Conrad et al., 1988; Montel and Vielzeuf, 1997) are shown for comparison. Related data are presented in Table S3.

(a) P-T pseudosection for the average Habahe Group volcanogenic components with calculated melt proportion isopleths. P-T conditions and compositions of the modelled melts are presented in Table 2. (b) Contents of representative oxides plotted versus pressure and temperature (see also Figs. S2, S3 and S4). (c) Whole-rock chemical projection for modelled melts from this study, partial melts modelled from terrigenous components of Jiang et al. (2016) and granitoids of the Chinese Altai are shown for comparison. (d) Multicationic A-B diagram after (Castro et al., 2010). Compositions of partial melts from melting experiments of quartz amphibolites (Patiño Douce and Beard, 1995), and metagreywackes (Conrad et al., 1988; Montel and Vielzeuf, 1997) are shown for comparison. Related data are presented in Table S3.

depleted in Nb, Ta and Ti (Fig. 7). Moreover, the generally positive $\varepsilon_{Nd}(400\,Ma)$ values of these studied intermediate-to-basic components, which are hard to distinguish from the variably depleted mantle-derived magmas in the region, further suggest that they are geochemically rather primitive. These findings advocate the view that the Habahe Group indeed does contain a significant amount of arc-related and geochemically primitive components as revealed in many previous studies (Cai et al., 2011a; Long et al., 2008; Sun et al., 2008; Windley et al., 2002). It is possible to envisage that partial melts originated from these components could inherit arc-like

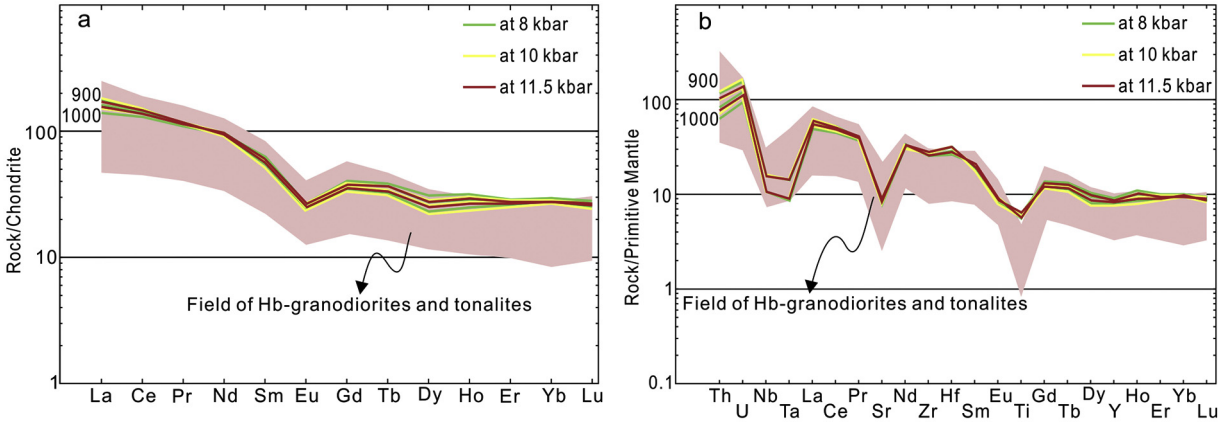

Fig. 7. Trace element modelling. (a) modelled chondrite normalized REE and (b) primitive mantle normalized trace element compositions of modelled melts equilibrated with amphibole + two-pyroxene + rutile + plagioclase at 900–1000 °C with melt fractions ranging from 15 to 35 vol%. For details see Analytical methods and Table S4.
Trace element modelling. (a) modelled chondrite normalized REE and (b) primitive mantle normalized trace element compositions of modelled melts equilibrated with amphibole + two-pyroxene + rutile + plagioclase at 900–1000 °C with melt fractions ranging from 15 to 35 vol%. For details see Analytical methods and Table S4.

trace element signatures as well as primitive geochemical characteristics. This idea is supported by the trace element modelling of melts that shows an excellent match with the published trace element compositions of the hornblende-granodiorites and tonalites in the region (Fig. 7). More interestingly, compared to most granitoids in the Chinese Altai, the volcanogenic components of the Habahe Group are chemically more radiogenic, while the terrigenous components of the Habahe Group are chemically less radiogenic, in terms of their Nd isotopic compositions (Fig. 5a). This is also advocated by the Nd model age as illustrated in Fig. 5b. As such, magma mixing in the source of these two components in various proportions could account for the Nd isotopic signatures of nearly all granitoids in the Chinese Altai. Such a model of magma in-source mixing could also explain the diversity of geochemical characteristics of the bulk Silurian-Devonian granitoids in the Chinese Altai which vary from peraluminous to metaluminous (Fig. 2c). We propose that the partial melts mainly derived from terrigenous components could potentially form typical "S-type" peraluminous granitoids whereas those originated predominantly from the investigated volcanogenic components could form typical "I-type" metaluminous granitoids (Fig. 8). This model is advocated also by the fact that most local granitoids formed rather peraluminous-to-metaluminous complexes in a short time period than a continuous diorite-tonalite-granodiorite-granitoid series exemplified by Cordilleran continental arcs (e.g., Ducea et al., 2003) or magmatic activities in the northerly Russian Gorny Altai (e.g., Kruk et al., 2011; Kruk, 2015). Indeed, the compositions of granitoids as well as their origin proposed in this work match well the typical S-type granites in circum-Pacific orogens, as described in Collins and Richards (2008). In conclusion, our findings therefore favor the idea that the volcanogenic components could potentially represent a chemically primitive source contributing to the formation of the granitoids in region. This model obviates the required significant contribution (70–90%) of the mantle-derived magmas envisaged in previous models (e.g., Wang et al., 2009).

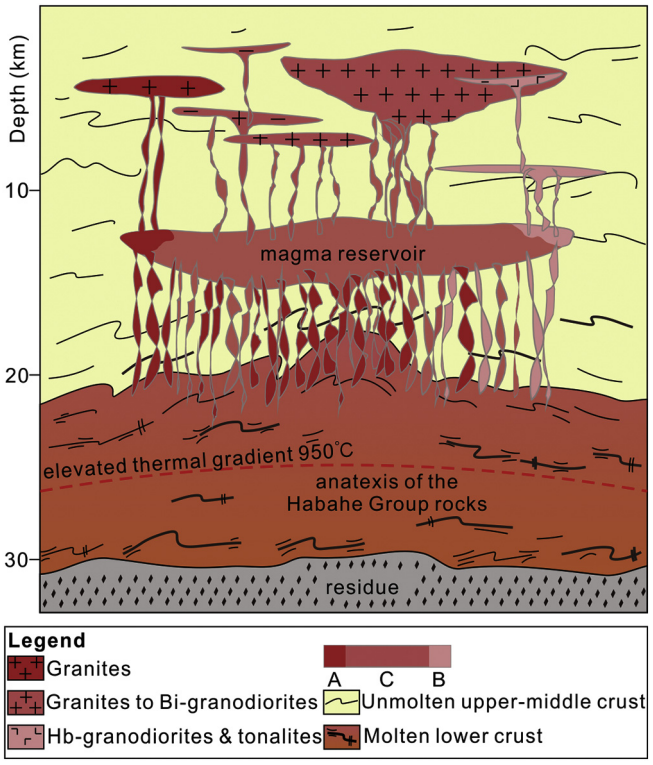

Fig. 8. A tentative model for the formation of the granitoids in the Chinese Altai (modified after Jiang et al., 2016). Horizontal axis is not to scale. "A": partial melts derived mainly from the terrigenous components of the Habahe Group; "B": partial melts derived predominantly from volcanogenic components of the Habahe Group; "C": in-source mixed partial melts from both terrigenous and volcanogenic components of the Habahe Group. It is shown that the dominant peraluminous granites to Bi-granodiorites are primarily originated from crustal magma from the anatexis of the Habahe Group rocks, the minor metaluminous Hb-granodiorites and tonalites are derived from the partial melts of the volcanogenic components of the Habahe Group. See text for detailed explanations.

6.2. Toward a better understanding of generation of hornblende-bearing I-type granitoids

Hornblende-bearing I-type granitoids dominate convergent margin batholiths. In many models, its emplacement reflects the transformation of juvenile mantle-derived mafic precursors into new felsic continental crust (Annen et al., 2008; Sisson et al., 2005). It has been proposed that primitive basaltic melts or a possibly initially more basaltic bulk arc crust can be differentiated toward evolved felsic continental crust through either extensive fractional crystallization or remelting (e.g., Anderson Jr, 1982; Annen et al., 2006; Holbrook et al., 1999; Lee and Bachmann, 2014; Rudnick, 1995). However, this is at odds with the substantial hybrid crust-mantle isotopic characteristics that are often found in I-type

granitoids (Bryant et al., 1997; Kemp et al., 2007; McCulloch and Chappell, 1982), suggesting derivation by remelting of supracrustal sedimentary or volcanogenic component. The question of whether the supracrustal component has been incorporated at depth, by interaction between crystallizing mantle-derived magmas and metasedimentary materials (e.g., Kemp et al., 2007) or via wholesale assimilation of metasedimentary wallrocks in the mid-crust by ascending I-type magmas (e.g., Collins, 1996) is still a subject of heated debate.

Relamination of deeply recycled felsic crustal material at the bottom of the arc crust has been introduced to explain the formation of granitoids with I-type chemical and isotopic signatures (e.g., Castro et al., 2013; Hacker et al., 2015). This view is advocated by the experimental findings and numerical modelling of Castro et al. (2010), who suggested that sub-lithospheric melting of greywacke-MORB mélanges could generate melts that are geochemically (major and trace elements) comparable with those of typical I-type granitoids at active continental margins. This may imply that growth of continental crust at convergent margins may take place by a net flux of primary silicic magmas with bulk tonalitic to granodioritic compositions, however, the applicability and details of depositing the mélanges at the base of the upper plate continental lithosphere still largely remain to be investigated. On the other hand, Hammerli et al. (2018) showed that open-system melt-rock interaction between metasedimentary-derived partial melt and heterogeneous lower crust could form magmas with I-type whole-rock chemical and isotopic signatures. This model does not require extensive melting of mafic protoliths, nor large input of mantle-derived magmas for mixing. In the current work, we show that the deeply buried intermediate-to-basic horizons or admixtures could be partially molten together with the interlayered terrigenous components during regional anatexis. At the attainable P-T conditions, these volcanogenic components could indeed produce a large amount of tonalitic to granodioritic magmas that chemically resemble the typical I-type hornblende-bearing granitoids (Fig. 6). In source magma mixing between the melts derived from interlayered intermediate-to-basic volcanogenic and terrigenous components could also explain variously hybrid whole-rock geochemical and isotopic variations commonly observed in I-type granitoids. In other words, the I-type granitoids could be mixtures of, rather than unique products from, different sources, and therefore they do not necessarily directly chemically image their source-rock compositions (Keay et al., 1997). Wedge sediments, especially those bearing high proportions of quartzofeldspathic components, are fertile in silicic melts and often of arc origin (Barker et al., 1992). Partial melting of fertile, heterogeneous wedge sediments can be an important mechanism contributing to the formation of I-type hornblende-bearing granitoids at convergent margins, by which direct infusion of mafic magma is un-necessary.

6.3. Implications for crustal growth in Altai accretionary system

The Chinese and Mongolian Altai represents a Cambrian to Ordovician sedimentary accretionary wedge that formed during the retreat of the Palaeo-Pacific subduction system (Jiang et al., 2017). This accretionary wedge extends from Russia, Kazakhstan, through China, to Mongolia, for >1500 km and is composed of detritus, eroded from pre-existing geological units to the west, together with accreted and imbricated ocean floor sediments and mafic volcanic rocks (Jiang et al., 2017; Xiao et al., 2009). A vast complexity of the crustal architecture is obvious. However, modern geophysical studies show that the deep structure of the Altai accretionary wedge featured a three-layer stratification of the crust typical of stable continents, i.e., a mafic granulite-facies lower crust and quartz-rich granitic middle and upper crust layers (Wang et al., 2003). Moreover, Bouguer anomalies across the Altai accretionary wedge also displayed horizontally heterogeneous signal marked by high-density lower crust in the southerly Chinese segment and low-density lower crust to the northerly Mongolian segment (Jiang et al., 2016). These characteristics indicate that the finite architecture of the Altai accretionary wedge is probably a result of crustal differentiation.

It is worth mentioning that a number of notable geological features, including regional-scale anatexis, emplacement of heterogeneous mafic rocks (Niu et al., 2006b; Wong et al., 2010) as well as extensive hydrothermal mineralization (Li et al., 2004b; Niu et al., 2006a) were coeval with the widespread intrusion of granitoids in the Chinese Altai. Compositionally heterogeneous mafic rocks, especially the association of adakite + high-Mg andesite + boninite + Nb-enriched basalt were taken as proxies of an abrupt change in the thermal regime attributed to upwelling of hot asthenospheric mantle (Cai et al., 2010; Niu et al., 2006b; Wong et al., 2010). Alternatively, asthenosphere upwelling associated with subduction of an active spreading oceanic ridge were proposed to explain the anomalous thermal conditions driving extensive crustal anatexis and magmatism in the region (Cai et al., 2010; Jiang et al., 2010; Sun et al., 2009). Crustal thinning above Pacific-type subduction systems was considered as the cause for massive melting of overriding fertile sediments in the Chinese Altai (Jiang et al., 2016), similar to that proposed for the generation of Circum-Pacific S-type granitoids by Collins and Richards (2008). Even though details regarding the exact mechanism accounting for the generation of these diagnostic geologic phenomena remain hotly debated, there seems a consensus that Middle Devonian anomalous thermal conditions associated with uncommonly elevated heat flux underneath the Chinese Altai is obvious.

The Devonian switching of thermal conditions could therefore account for the regional-scale anatexis in the Chinese Altai (Jiang et al., 2010). The close temporal and spatial relationship between the formation of granitoids and regional anatexis of the Habahe Group, as well as their geochemical similarities, as exemplified in this study and the previous work of Jiang et al. (2016), allow the conclusion that the Silurian-Devonian granitoids originated from the partial melting of the Habahe Group, an amplification of regional-scale crustal anatexis in the Chinese Altai (Jiang et al., 2010, 2015). As a result, the extensive partial melting of the Habahe Group metasediments would lead to large-scale differentiation of the crust through extraction and ascent of felsic melt to middle and upper crustal levels, leaving a dense and refractory lower crust. Such a process can well explain the three-layered crustal architecture of the Chinese Altai. Recent structural and geochronological database revealed that the Chinese Altai was affected by horizontal flow of partially molten lower crust dated at about 390 Ma (Broussolle et al., 2019; Zhang et al., 2015). Formation of sub-horizontal sheeted granites was also reported from the neighboring Mongolian Altai, with Middle Devonian ages (Hanžl et al., 2016; Lehmann et al., 2017). All those have been interpreted as the result of orogen-scale horizontal extension and vertical shortening. Such a process probably represents a potentially viable model for redistribution of accretionary mass and modified geophysical signals in general. Collectively, our results suggest that partial melting of the Altai accretionary wedge could promote the further crustal differentiation and eventually can transform homogeneous crustal architecture into a vertically stratified one. This process may be a key mechanism contributing to the stabilization and peripheral growth of continental crust of accretionary system worldwide.

7. Conclusions

Geological and geochemical data, phase equilibrium and trace element modelling are combined to characterize the formation of

hornblende-bearing I-type granitoids in the Chinese Altai. The principal conclusions are as follows:

1. A large amount of intermediate-to-basic component is preserved in the Habahe Group sedimentary succession. This component is characterized by arc-related geochemical affinities and primitive isotopic signatures.
2. Partial melting of the volcanogenic component at 900–1000 °C can produce about 30–35 vol% silicic melts that show a good chemical match of major and trace element with those of the I-type granitoids in the Chinese Altai. We suggest that Silurian-Devonian hornblende-bearing I-type granitoids could be originated from the intermediate-to-basic volcanogenic components and the requirement of significant input of mantle-derived magma envisaged previously is un-necessary.
3. Peripheral growth of continental crust at convergent margins is not necessary to be attained only by arc magmatism. Anatexis of the accretionary wedge can serve as another viable mechanism contributing to the transformation of accretionary wedges into stabilized and vertically stratified continental crust in accretionary orogens worldwide.

Supplementary data to this article can be found online at https://doi.org/10.1016/j.gr.2019.07.019.

Acknowledgments

This work was supported by the National Key Research and Development Program of China (Grant No. 2017YFC0601205), Strategic Priority Research Program (B) of the CAS (XDB18020203), NSF China (41672056 and 41872222), the Czech Science Foundation (GACR grant EXPRO 19-27682X), and GIG-CAS 135 project 135TP201601. The Guangdong Special Support Program to Y.D.J. and the Thousand Youth Talents Plan to P.F.L. are also acknowledged. Dr. Yu Yang is thanked for his valuable comments on an earlier version of this manuscript. Constructive reviews from associate Editor Andrea Festa and another anonymous reviewer resulted in significant improvements to the paper.

References

Allègre, C.J., Othman, D.B., 1980. Nd–Sr isotopic relationship in granitoid rocks and continental crust development: a chemical approach to orogenesis. Nature 286, 335.
Anderson, Jr, A.T., 1982. Parental basalts in subduction zones: implications for continental evolution. J. Geophys. Res. Solid Earth 87, 7047–7060.
Annen, C., Blundy, J.D., Sparks, R.S.J., 2006. The genesis of intermediate and silicic magmas in deep crustal hot zones. J. Petrol. 47, 505–539.
Annen, C., Blundy, J.D., Sparks, R.S.J., 2008. The sources of granitic melt in deep hot zones. Trans. R. Soc. Edinb. Earth Sci. 97, 297–309.
Badarch, G., Cunningham, W.D., Windley, B.F., 2002. A new terrane subdivision for Mongolia: implications for the Phanerozoic crustal growth of Central Asia. J. Asian Earth Sci. 21, 87–110.
Barker, F., Farmer, G.L., Ayuso, R.A., Plafker, G., Lull, J.S., 1992. The 50 Ma granodiorite of the eastern Gulf of Alaska: melting in an accretionary prism in the forearc. J. Geophys. Res. Solid Earth 97, 6757–6778.
Bhatia, M.R., Crook, K.A.W., 1986. Trace-element characteristics of graywackes and tectonics setting discrimination of sedimentary basins. Contrib. Mineral. Petrol. 92, 181–193.
Broussolle, A., Aguilar, C., Sun, M., Schulmann, K., Štípská, P., Jiang, Y., Yu, Y., Xiao, W., Wang, S., Míková, J., 2018. Polycyclic Palaeozoic evolution of accretionary orogenic wedge in the southern Chinese Altai: evidence from structural relationships and U–Pb geochronology. Lithos 314-315, 400–424.
Broussolle, A., Sun, M., Schulmann, K., Guy, A., Aguilar, C., Štípská, P., Jiang, Y.D., Yu, Y., Xiao, W.J., 2019. Are the Chinese Altai "terranes" the result of juxtaposition of different crustal levels during Late Devonian and Permian orogenesis? Gondwana Res. 66, 183–206.
Bryant, C.J., Arculus, R.J., Chappell, B.W., 1997. Clarence river supersuite: 250 Ma Cordilleran tonalitic I-type intrusions in eastern Australia. J. Petrol. 38, 975–1001.
Buriánek, D., Schulmann, K., Hrdličková, K., Hanžl, P., Janoušek, V., Gerdes, A., Lexa, O., 2017. Geochemical and geochronological constraints on distinct early-Neoproterozoic and Cambrian accretionary events along southern margin of the Baydrag continent in western Mongolia. Gondwana Res. 47, 200–227.
Cai, K.D., Sun, M., Yuan, C., Zhao, G.C., Xiao, W.J., Long, X.P., Wu, F.Y., 2010. Geochronological and geochemical study of mafic dykes from the northwest Chinese Altai: implications for petrogenesis and tectonic evolution. Gondwana Res. 18, 638–652.
Cai, K.D., Sun, M., Yuan, C., Long, X.P., Xiao, W.J., 2011. Geological framework and Paleozoic tectonic history of the Chinese Altai, NW China: a review. Russ. Geol. Geophys. 52, 1619–1633.
Cai, K.D., Sun, M., Yuan, C., Zhao, G.C., Xiao, W.J., Long, X.P., Wu, F.Y., 2011. Prolonged magmatism, juvenile nature and tectonic evolution of the Chinese Altai, NW China: evidence from zircon U–Pb and Hf isotopic study of Paleozoic granitoids. J. Asian Earth Sci. 42, 949–968.
Castro, A., Gerya, T., Garcia-Casco, A., Fernandez, C., Diaz-Alvarado, J., Moreno-Ventas, I., Low, I., 2010. Melting relations of MORB–sediment mélanges in underplated mantle wedge plumes; implications for the origin of cordilleran-type batholiths. J. Petrol. 51, 1267–1295.
Castro, A., Vogt, K., Gerya, T., 2013. Generation of new continental crust by sub-lithospheric silicic-magma relamination in arcs: a test of Taylor's andesite model. Gondwana Res. 23, 1554–1566.
Cawood, P.A., Kröner, A., Collins, W.J., Kusky, T.M., Mooney, W.D., Windley, B.F., 2009. Accretionary orogens through Earth history. Geol. Soc. Lond., Spec. Publ. 318, 1–36.
Chappell, B.W., Bryant, C.J., Wyborn, D., 2012. Peraluminous I-type granites. Lithos 153, 142–153.
Chen, B., Jahn, B.M., 2002. Geochemical and isotopic studies of the sedimentary and granitic rocks of the Altai orogen of northwest China and their tectonic implications. Geol. Mag. 139, 1–13.
Collett, S., Stipska, P., Schulmann, K., Peresty, V., Soldner, J., Anczkiewicz, R., Lexa, O., Kylander-Clark, A., 2018. Combined Lu-Hf and Sm-Nd geochronology of the Marianske Lazne Complex: new constraints on the timing of eclogite- and granulite-facies metamorphism. Lithos 304, 74–94.
Collins, W.J., 1996. Lachlan Fold Belt granitoids: products of three-component mixing. Trans. R. Soc. Edinb. Earth Sci. 87, 171–181.
Collins, W.J., Richards, S.W., 2008. Geodynamic significance of S-type granites in circum-Pacific orogens. Geology 36, 559–562.
Condie, K.C., 1997. Plate Tectonics and Crustal Evolution, Fourth edition. Butterworth Heinemann.
Condie, K.C., Noll, P.D., Conway, C.M., 1992. Geochemical and detrital mode evidence for 2 sources of early proterozoic sedimentary-rocks from the Tonto basins supergroup, central Arizona. Sediment. Geol. 77, 51–76.
Conrad, W.K., Nicholls, I.A., Wall, V.J., 1988. Water-saturated and -undersaturated melting of metaluminous and peraluminous crustal compositions at 10 kb: evidence for the origin of silicic magmas in the Taupo Volcanic Zone, New Zealand, and other occurrences. J. Petrol. 29, 765–803.
Debon, F., 1983. A chemical-mineralogical classification of common plutonic rocks and associations. Trans. R. Soc. Edinb. Earth Sci. 73, 135–149.
DePaolo, D.J., 1981. A neodymium and strontium isotopic study of the Mesozoic calc-alkaline granitic batholiths of the Sierra Nevada and Peninsular Ranges, California. J. Geophys. Res. Solid Earth 86, 10470–10488.
Ducea, M.N., Kidder, S., Zandt, G., 2003. Arc composition at mid-crustal depths: insights from the Coast Ridge Belt, Santa Lucia Mountains, California. Geophys. Res. Lett. (13).
Gerya, T.V., Connolly, J.A.D., Yuen, D.A., Gorczyk, W., Capel, A.M., 2006. Seismic implications of mantle wedge plumes. Phys. Earth Planet. Inter. 156, 59–74.
Gladkochub, D.P., Donskaya, T.V., Wingate, M.T.D., Poller, U., Kröner, A., Fedorovsky, V.S., Mazukabzov, A.M., Todt, W., Pisarevsky, S.A., 2008. Petrology, geochronology, and tectonic implications of c. 500 Ma metamorphic and igneous rocks along the northern margin of the central Asian orogen (Olkhon terrane, Lake Baikal, Siberia). J. Geol. Soc. 165 (1), 235–246.
Glorie, S., De Grave, J., Buslov, M.M., Zhimulev, F.I., Safonova, I.Y., 2014. Detrital zircon provenance of early Palaeozoic sediments at the southwestern margin of the Siberian Craton: insights from U–Pb geochronology. J. Asian Earth Sci. 82, 115–123.
Gorczyk, W., Gerya, T.V., Connolly, J.A.D., Yuen, D.A., 2007. Growth and mixing dynamics of mantle wedge plumes. Geology 35, 587–590.
Green, E.C.R., White, R.W., Diener, J.F.A., Powell, R., Holland, T.J.B., Palin, R.M., 2016. Activity-composition relations for the calculation of partial melting equilibria in metabasic rocks. J. Metamorph. Geol. 34, 845–869.
Gu, X.X., Liu, J.M., Zheng, M.H., Tang, J.X., Qi, L., 2002. Provenance and tectonic setting of the Proterozoic turbidites in Hunan, South China: geochemical evidence. J. Sediment. Res. 72, 393–407.
Hacker, B.R., Kelemen, P.B., Behn, M.D., 2015. Continental lower crust. Annu. Rev. Earth Planet. Sci. 43, 167–205.
Hammerli, J., Kemp, A.I.S., Shimura, T., Vervoort, J.D., Dunkley, D.J., Eimf, 2018. Generation of I-type granitic rocks by melting of heterogeneous lower crust. Geology 46, 907–910.
Hanžl, P., Schulmann, K., Janoušek, V., Lexa, O., Hrdličková, K., Jiang, Y.D., Buriánek, D., Altanbaatar, B., Ganchuluun, T., Erban, V., 2016. Making continental crust: origin of Devonian orthogneisses from SE Mongolian Altai. J. Geosci. 61, 25–50.
Hawkesworth, C.J., Dhuime, B., Pietranik, A.B., Cawood, P.A., Kemp, A.I.S., Storey, C.D., 2010. The generation and evolution of the continental crust. J. Geol. Soc. 167, 229–248.
Holbrook, W.S., Lizarralde, D., McGeary, S., Bangs, N., Diebold, J., 1999. Structure and composition of the Aleutian island arc and implications for continental crustal growth. Geology 27, 31–34.

Holland, T., Powell, R., 2003. Activity-composition relations for phases in petrological calculations: an asymmetric multicomponent formulation. Contrib. Mineral. Petrol. 145, 492–501.
Holland, T.J.B., Powell, R., 2011. An improved and extended internally consistent thermodynamic dataset for phases of petrological interest, involving a new equation of state for solids. J. Metamorph. Geol. 29, 333–383.
Huang, Y.Q., Jiang, Y.D., Yu, Y., Collet, S., Wang, S., Shu, T., Xu, K., 2019. Nd-Hf isotopic decoupling of the Silurian-Devonian granitoids in the Chinese Altai: a consequence of crustal recycling of the Ordovician accretionary wedge? J. Earth Sci. doi:10.1007/s12583-019-1217-x.
Irvine, T.N., Baragar, W.R.A., 1971. A guide to the chemical classification of the common volcanic rocks. Can. J. Earth Sci. 8, 523–548.
Jahn, B.-m., Wu, F., Chen, B., 2000. Granitoids of the Central Asian Orogenic Belt and continental growth in the Phanerozoic. In: Barbarin, B., Stephens, W.E., Bonin, B., Bouchez, J.-L., Clarke, D.B., Cuney, M., Martin, H. (Eds.), The Fourth Hutton Symposium on the Origin of Granites and Related Rocks. Geological Society of America.
Janoušek, V., Jiang, Y.D., Burianek, D., Schulmann, K., Hanzl, P., Soejono, I., Kroner, A., Altanbaatar, B., Erban, V., Lexa, O., Ganchuluun, T., Kosler, J., 2018. Cambrian-Ordovician magmatism of the Ikh-Mongol Arc System exemplified by the Khantaishir Magmatic Complex (Lake Zone, south-central Mongolia). Gondwana Res. 54, 122–149.
Jiang, Y.D., Sun, M., Zhao, G.C., Yuan, C., Xiao, W.J., Xia, X.P., Long, X.P., Wu, F.Y., 2010. The ~390 Ma high-T metamorphic event in the Chinese Altai: a consequence of ridge-subduction? Am. J. Sci. 310, 1421–1452.
Jiang, Y.D., Sun, M., Zhao, G.C., Yuan, C., Xiao, W.J., Xia, X.P., Long, X.P., Wu, F.Y., 2011. Precambrian detrital zircons in the Early Paleozoic Chinese Altai: their provenance and implications for the crustal growth of central Asia. Precambrian Res. 189, 140–154.
Jiang, Y.D., Štípská, P., Sun, M., Schulmann, K., Zhang, J., Wu, Q.H., Long, X.P., Yuan, C., Racek, M., Zhao, G.C., 2015. Juxtaposition of Barrovian and migmatite domains in the Chinese Altai: a result of crustal thickening followed by doming of partially molten lower crust. J. Metamorph. Geol. 33, 45–70.
Jiang, Y.D., Schulmann, K., Sun, M., Štípská, P., Guy, A., Janoušek, V., Lexa, O., Yuan, C., 2016. Anatexis of accretionary wedge, Pacific-type magmatism, and formation of vertically stratified continental crust in the Altai Orogenic Belt. Tectonics 35, 3095–3118.
Jiang, Y.D., Schulmann, K., Kroener, A., Sun, M., Lexa, O., Janousek, V., Burianek, D., Yuan, C., Hanzl, P., 2017. Neoproterozoic-Early Paleozoic peri-Pacific accretionary evolution of the Mongolian collage system: insights from geochemical and U-Pb zircon data from the Ordovician sedimentary wedge in the Mongolian Altai. Tectonics 36, 2305–2331.
Jiang, Y.D., Schulmann, K., Sun, M., Weinberg, R.F., Atípská, P., Li, P.F., Zhang, J., Chopin, F., Wang, S., Xia, X.P., Xiao, W.J., 2019. Structural and geochronological constraints on Devonian suprasubduction tectonic switching and Permian collisional dynamics in the Chinese Altai, Central Asia. Tectonics 38, 253–280.
Keay, S., Collins, W.J., McCulloch, M.T., 1997. A three-component Sr-Nd isotopic mixing model for granitoid genesis, Lachlan fold belt, eastern Australia. Geology 25, 307–310.
Kemp, A.I.S., Hawkesworth, C.J., Foster, G.L., Paterson, B.A., Woodhead, J.D., Hergt, J.M., Gray, C.M., Whitehouse, M.J., 2007. Magmatic and crustal differentiation history of granitic rocks from Hf-O isotopes in zircon. Science 315, 980–983.
Kröner, A., Windley, B.F., Badarch, G., Tomurtogoo, O., Hegner, E., Jahn, B.M., Gruschka, S., Khain, E.V., Demoux, A., Wingate, M.T.D., 2007. Accretionary growth and crust-formation in the Central Asian Orogenic Belt and comparison with the Arbian-Nubian shield. In: Hatcher, J.R.D., Carlson, M.P., McBride, J.H., Catalán, J.R.M. (Eds.), 4-D Framework of Continental Crust. Geological Society of America.
Kröner, A., Kovach, V., Alexeiev, D., Wang, K.-L., Wong, J., Degtyarev, K., Kozakov, I., 2017. No excessive crustal growth in the Central Asian Orogenic Belt: further evidence from field relationships and isotopic data. Gondwana Res. 50, 135–166.
Kruk, N.N., 2015. Continental crust of Gorny Altai: stages of formation and evolution; indicative role of granitoids. Russ. Geol. Geophys. 56, 1097–1113.
Kruk, N.N., Rudnev, S.N., Vladimirov, A.G., Shokalsky, S.P., Kovach, V.P., Serov, P.A., Volkova, N.I., 2011. Early–Middle Paleozoic granitoids in Gorny Altai, Russia: implications for continental crust history and magma sources. J. Asian Earth Sci. 42, 928–948.
Kruk, N.N., Kuibida, Y.V., Shokalsky, S.P., Kiselev, V.I., Gusev, N.I., 2018. Late Cambrian – Early Ordovician turbidites of Gorny Altai (Russia): compositions, sources, deposition settings, and tectonic implications. J. Asian Earth Sci. 159, 209–232.
Kuzmichev, A.B., 2015. Neoproterozoic accretion of the Tuva-Mongolian massif, one of the Precambrian terranes in the Central Asian Orogenic Belt. In: Kröner, A. (Ed.), Composition and Evolution of Central Asian Orogenic Belt: Geology, Evolution, Tectonics and Models. Bornträger Science Publishers, Stuttgart, pp. 66–92.
Laurent-Charvet, S., Charvet, J., Monié, P., Shu, L., 2003. Late Paleozoic strike-slip shear zones in eastern central Asia (NW China): new structural and geochronological data. Tectonics 22.
Le Maitre, R.W., Bateman, P., Dudek, A., Keller, J., Le Bas, M.J., Sabine, P.A., Schmid, R., Sorensen, H., Streckeisen, A., Woolley, A.R., Zanettin, B., 1989. A Classification of Igneous Rocks and Glossary of Terms. Blackwell, Oxford, pp. 1–193.
Lee, C.-T.A., Bachmann, O., 2014. How important is the role of crystal fractionation in making intermediate magmas? Insights from Zr and P systematics. Earth Planet. Sci. Lett. 393, 266–274.
Lehmann, J., Schulmann, K., Lexa, O., Závada, P., Štípská, P., Hasalová, P., Belyanin, G., Corsini, M., 2017. Detachment folding of partially molten crust in accretionary orogens: a new magma-enhanced vertical mass and heat transfer mechanism. Lithosphere 9, 889–909.
Lexa, O., 2017. PyPSbuilder – simplistic THERMOCALC front-end for constructing PT pseudosections (v.2.1.3.). Accessed date: September 2017, Available at: https://github.com/ondrolexa/pypsbuilder.
Li, X.H., Zhou, H.W., Chung, S.L., Lo, C.H., Wei, G.J., Liu, Y., Lee, C.Y., 2002. Geochemical and Sr-Nd isotopic characteristics of Late Paleogene ultrapotassic magmatism in Southeastern Tibet. Int. Geol. Rev. 44, 559–574.
Li, X.H., Liu, D.Y., Sun, M., Li, W.X., Liang, X.R., Liu, Y., 2004. Precise Sm–Nd and U–Pb isotopic dating of the supergiant Shizhuyuan polymetallic deposit and its host granite, SE China. Geol. Mag. 141, 225–231.
Li, Z.L., Chen, H.L., Yang, S.F., Xiao, W.J., Tainosho, Y., 2004. Discovery of mafic granulites from the Altay orogenic belt; evidence from mineralogical study. Acta Petrol. Sin. 20, 1445–1455.
Li, X.H., Qi, C.S., Liu, Y., Liang, X.R., Tu, X.L., Xie, L., Yang, Y.H., 2005. Petrogenesis of the Neoproterozoic bimodal volcanic rocks along the western margin of the Yangtze Block: new constraints from Hf isotopes and Fe/Mn ratios. Chin. Sci. Bull. 2481–2486.
Li, X.H., Li, Z.X., Li, W.X., Liu, Y., Yuan, C., Wei, G.J., Qi, C.S., 2007. U–Pb zircon, geochemical and Sr–Nd–Hf isotopic constraints on age and origin of Jurassic I- and A-type granites from central Guangdong, SE China: a major igneous event in response to foundering of a subducted flat-slab? Lithos 96, 186–204.
Li, Z.L., Yang, X.Q., Li, Y.Q., Santosh, M., Chen, H.L., Xiao, W.J., 2014. Late Paleozoic tectono–metamorphic evolution of the Altai segment of the Central Asian Orogenic Belt: constraints from metamorphic P–T pseudosection and zircon U–Pb dating of ultra-high-temperature granulite. Lithos 204, 83–96.
Li, P.F., Sun, M., Rosenbaum, G., Cai, K.D., Yu, Y., 2015. Structural evolution of the Irtysh Shear Zone (northwestern China) and implications for the amalgamation of arc systems in the Central Asian Orogenic Belt. J. Struct. Geol. 80, 142–156.
Li, P.F., Sun, M., Rosenbaum, G., Jourdan, F., Li, S.Z., Cai, K.D., 2017. Late Paleozoic closure of the Ob-Zaisan Ocean along the Irtysh shear zone (NW China): implications for arc amalgamation and oroclinal bending in the Central Asian orogenic belt. GSA Bull. 129, 547–569.
Liu, W., Liu, X.J., Xiao, W.J., 2012. Massive granitoid production without massive continental-crust growth in the Chinese Altay: insight into the source rock of granitoids using integrated zircon U-Pb age, Hf-Nd-Sr isotopes and geochemistry. Am. J. Sci. 312, 629–684.
Long, X.P., Sun, M., Yuan, C., Xiao, W.J., Lin, S.F., Wu, F.Y., Xia, X.P., Cai, K.D., 2007. Detrital zircon age and Hf isotopic studies for metasedimentary rocks from the Chinese Altai: implications for the Early Paleozoic tectonic evolution of the Central Asian Orogenic Belt. Tectonics 26.
Long, X.P., Sun, M., Yuan, C., Xiao, W.J., Cai, K.D., 2008. Early Paleozoic sedimentary record of the Chinese Altai: implications for its tectonic evolution. Sediment. Geol. 208, 88–100.
Long, X.P., Yuan, C., Sun, M., Xiao, W.J., Zhao, G.C., Wang, Y.J., Cai, K.D., Xia, X.P., Xie, L.W., 2010. Detrital zircon ages and Hf isotopes of the early Paleozoic flysch sequence in the Chinese Altai, NW China: new constrains on depositional age, provenance and tectonic evolution. Tectonophysics 480, 213–231.
Long, X.P., Yuan, C., Sun, M., Xiao, W.J., Wang, Y.J., Cai, K.D., Jiang, Y.D., 2012. Geochemistry and Nd isotopic composition of the Early Paleozoic flysch sequence in the Chinese Altai, Central Asia: evidence for a northward-derived mafic source and insight into Nd model ages in accretionary orogen. Gondwana Res. 22, 554–566.
McCulloch, M.T., Chappell, B.W., 1982. Nd isotopic characteristics of S- and I-type granites. Earth Planet. Sci. Lett. 58, 51–64.
McCulloch, M.T., Gamble, J.A., 1991. Geochemical and geodynamical constraints on subduction zone magmatism. Earth Planet. Sci. Lett. 102, 358–374.
McLennan, S.M., Taylor, S.R., McGregor, V.R., 1984. Geochemistry of Archean metasedimentary rocks from West Greenland. Geochim. Cosmochim. Acta 48, 1–13.
Montel, J.M., Vielzeuf, D., 1997. Partial melting of metagreywackes, part II. Compositions of minerals and melts. Contrib. Mineral. Petrol. 128, 176–196.
Niu, H.C., Sato, H., Zhang, H.X., Ito, J., Yu, X.Y., Nagao, T., Terada, K., Zhang, Q., 2006. Juxtaposition of adakite, boninite, high-TiO2 and low-TiO2 basalts in the Devonian southern Altay, Xinjiang, NW China. J. Asian Earth Sci. 28, 439–456.
Niu, H.C., Yu, X.Y., Xu, J.F., 2006. Late Paleozoic Volcanism and Associated Metallogenesis in the Altay Area, Xinjiang, China. Geological Publishing House, Beijing.
Patiño Douce, A.E., Beard, J.S., 1995. Dehydration-melting of biotite gneiss and quartz amphibolite from 3 to 15 kbar. J. Petrol. 36, 707–738.
Pettijohn, F.J., Potter, P.E., Siever, R., 1987. Sand and Sandstone, 2nd ed. Springer, New York.
Powell, R., Holland, T.J.B., 1988. An internally consistent dataset with uncertainties and correlations: 3. Applications to geobarometry, worked examples and a computer program. J. Metamorph. Geol. 6, 173–204.
Priyatkina, N., Khudoley, A.K., Collins, W.J., Kuznetsov, N.B., Huang, H.Q., 2016. Detrital zircon record of Meso- and Neoproterozoic sedimentary basins in northern part of the Siberian Craton: characterizing buried crust of the basement. Precambrian Res. 285, 21–38.
Rebay, G., Powell, R., Diener, J.F.A., 2010. Calculated phase equilibria for a morb composition in a P-T range, 450–650 degrees C and 18–28 kbar: the stability of eclogite. J. Metamorph. Geol. 28, 635–645.
Rudnick, R.L., 1995. Making continental crust. Nature 378, 571–578.
Rutter, M.J., Wyllie, P.J., 1988. Melting of vapour-absent tonalite at 10 kbar to

simulate dehydration–melting in the deep crust. Nature 331, 159.
Safonova, I., 2017. Juvenile versus recycled crust in the Central Asian Orogenic Belt: implications from ocean plate stratigraphy, blueschist belts and intra-oceanic arcs. Gondwana Res. 47, 6–27.
Safonova, I.Y., Utsunomiya, A., Kojima, S., Nakae, S., Tomurtogoo, O., Filippov, A.N., Koizumi, K., 2009. Pacific superplume-related oceanic basalts hosted by accretionary complexes of Central Asia, Russian Far East and Japan. Gondwana Res. 16, 587–608.
Schilling, J.G., Zajac, M., Evans, R., Johnston, T., White, W., Devine, J.D., Kingsley, R., 1983. Petrologic and geochemical variations along the mid-Atalantic ridge from 29-degrees-N to 73-degrees-N. Am. J. Sci. 283, 510–586.
Şengör, A.M.C., Natalin, B.A., 1996. Turkic-type orogeny and its role in the making of the continental crust. Annu. Rev. Earth Planet. Sci. 24, 263–337.
Şengör, A.M.C., Natal'in, B.A., Burtman, V.S., 1993. Evolution of the Altaid tectonic collage and Palaeozoic crustal growth in Eurasia. Nature 364, 299.
Sisson, T.W., Ratajeski, K., Hankins, W.B., Glazner, A.F., 2005. Voluminous granitic magmas from common basaltic sources. Contrib. Mineral. Petrol. 148, 635–661.
Soejono, I., Buriánek, D., Svojtka, M., Žáček, V., Čáp, P., Janoušek, V., 2016. Mid-Ordovician and late Devonian magmatism in the Togtokhinshil complex: new insight into the formation and accretionary evolution of the Lake zone (western Mongolia). J. Geosci. 61 (1), 5–23.
Solano, J.M.S., Jackson, M.D., Sparks, R.S.J., Blundy, J.D., Annen, C., 2012. Melt segregation in deep crustal hot zones: a mechanism for chemical differentiation, crustal assimilation and the formation of evolved magmas. J. Petrol. 53, 1999–2026.
Štípská, P., Schulmann, K., Lehmann, J., Corsini, M., Lexa, O., Tomurhuu, D., 2010. Early Cambrian eclogites in SW Mongolia: evidence that the Palaeo-Asian Ocean suture extends further east than expected. J. Metamorph. Geol. 28, 915–933.
Sun, S.S., Mcdonough, W.F., 1989. Chemical and isotopic systematics of oceanic basalts: implications for mantle composition and processes. Geol. Soc. Lond. Spec. Publ. 42, 313–345.
Sun, M., Yuan, C., Xiao, W.J., Long, X.P., Xia, X.P., Zhao, G.C., Lin, S.F., Wu, F.Y., Kröner, A., 2008. Zircon U-Pb and Hf isotopic study of gneissic rocks from the Chinese Altai: progressive accretionary history in the early to middle Palaeozoic. Chem. Geol. 247, 352–383.
Sun, M., Long, X.P., Cai, K.D., Jiang, Y.D., Wang, B.Y., Chao, Y., Zhao, G.C., Xiao, W.J., Wu, F.Y., 2009. Early Paleozoic ridge subduction in the Chinese Altai: insight from the abrupt change in zircon Hf isotopic compositions. Sci. China Ser. D Earth Sci. 52, 1345–1358.
Taylor, S.R., 1967. The origin and growth of continents. Tectonophysics 4, 17–34.
Tong, Y., Wang, T., Hong, D.W., Dai, Y.J., Han, B.F., Liu, X.M., 2007. Ages and origin of the early Devonian granites from the north part of Chinese Altai Mountains and its tectonic implications. Acta Petrol. Sin. 23, 1933–1944.
Villaseca, C., Barbero, L., Herreros, V., 1998. A re-examination of the typology of peraluminous granite types in intracontinental orogenic belts. Trans. R. Soc. Edinb. Earth Sci. 89, 113–119.
Wang, Y.X., Mooney, W.D., Yuan, X.C., Coleman, R.G., 2003. The crustal structure from the Altai Mountains to the Altyn Tagh fault, northwest China. J. Geophys. Res. Solid Earth 108.
Wang, T., Hong, D.W., Jahn, B.M., Tong, Y., Wang, Y.B., Han, B.F., Wang, X.X., 2006. Timing, petrogenesis, and setting of Paleozoic synorogenic intrusions from the Altai Mountains, Northwest China: implications for the tectonic evolution of an accretionary orogen. J. Geol. 114, 735–751.
Wang, T., Jahn, B.M., Kovach, V.P., Tong, Y., Hong, D.W., Han, B.F., 2009. Nd–Sr isotopic mapping of the Chinese Altai and implications for continental growth in the Central Asian Orogenic Belt. Lithos 110, 359–372.
Wei, C.J., Clarke, G., Tian, W., Qiu, L., 2007. Transition of metamorphic series from the kyanite- to andalusite-types in the Altai orogen, Xinjiang, China: evidence from petrography and calculated KMnFMASH and KFMASH phase relations. Lithos 96, 353–374.
White, R.W., Powell, R., Holland, T.J.B., Worley, B.A., 2000. The effect of TiO2 and Fe2O3 on metapelitic assemblages at greenschist and amphibolite facies conditions: mineral equilibria calculations in the system K2O-FeO-MgO-Al2O3-SiO2-H2O-TiO2-Fe2O3. J. Metamorph. Geol. 18, 497–511.
White, R.W., Powell, R., Clarke, G.L., 2002. The interpretation of reaction textures in Fe-rich metapelitic granulites of the Musgrave Block, central Australia: constraints from mineral equilibria calculations in the system K2O-FeO-MgO-Al2O3-SiO2-H2O-TiO2-Fe2O3. J. Metamorph. Geol. 20, 41–55.
White, R.W., Powell, R., Holland, T.J.B., Johnson, T.E., Green, E.C.R., 2014. New mineral activity-composition relations for thermodynamic calculations in metapelitic systems. J. Metamorph. Geol. 32, 261–286.
Wilhem, C., Windley, B.F., Stampfli, G.M., 2012. The Altaids of Central Asia: a tectonic and evolutionary innovative review. Earth Sci. Rev. 113, 303–341.
Windley, B.F., Kröner, A., Guo, J., Qu, G., Li, Y., Zhang, C., 2002. Neoproterozoic to Paleozoic geology of the Altai Orogen, NW China: new zircon age data and tectonic evolution. J. Geol. 110, 719–737.
Windley, B.F., Alexeiev, D., Xiao, W.J., Kröner, A., Badarch, G., 2007. Tectonic models for accretion of the Central Asian Orogenic Belt. J. Geol. Soc. 164, 31–47.
Wolf, M.B., Wyllie, P.J., 1994. Dehydration-melting of amphibolite at 10 kbar: the effects of temperature and time. Contrib. Mineral. Petrol. 115, 369–383.
Wong, K., Sun, M., Zhao, G.C., Yuan, C., Xiao, W.J., 2010. Geochemical and geochronological studies of the Alegedayi Ophiolitic Complex and its implication for the evolution of the Chinese Altai. Gondwana Res. 18, 438–454.
Wyllie, P.J., 1977. Crustal anatexis: an experimental review. Tectonophysics 43, 41–71.
Xiao, W.J., Windley, B.F., Badarch, G., Sun, S., Li, J.L., Qin, K., Wang, Z., 2004. Palaeozoic accretionary and convergent tectonics of the southern Altaids: implications for the growth of Central Asia. J. Geol. Soc. 161, 339–342.
Xiao, W.J., Windley, B.F., Yuan, C., Sun, M., Han, C.M., Lin, S.F., Chen, H.L., Yan, Q.R., Liu, D.Y., Qin, K.Z., Li, J.L., Sun, S., 2009. Paleozoic multiple subduction-accretion processes of the southern Altaids. Am. J. Sci. 309, 221–270.
Xiao, W.J., Huang, B.C., Han, C.M., Sun, S., Li, J.L., 2010. A review of the western part of the Altaids: a key to understanding the architecture of accretionary orogens. Gondwana Res. 18, 253–273.
Yu, Y., Sun, M., Huang, X.L., Zhao, G., Li, P.F., Long, X.P., Cai, K.D., Xia, X.P., 2017. Sr-Nd-Hf-Pb isotopic evidence for modification of the Devonian lithospheric mantle beneath the Chinese Altai. Lithos 284-285, 207–221.
Yu, Y., Sun, M., Long, X.P., Li, P.F., Zhao, G.C., Kröner, A., Broussolle, A., Yang, J.H., 2017. Whole-rock Nd–Hf isotopic study of I-type and peraluminous granitic rocks from the Chinese Altai: constraints on the nature of the lower crust and tectonic setting. Gondwana Res. 47, 131–141.
Yu, Y., Sun, M., Yuan, C., Zhao, G.C., Huang, X.L., Rojas-Agramonte, Y., Chen, Q., 2018. Evolution of the middle Paleozoic magmatism in the Chinese Altai: Constraints on the crustal differentiation at shallow depth in the accretionary orogen. Journal of Asian Earth Sciences 175, 230–246.
Yuan, C., Sun, M., Xiao, W.J., Li, X.H., Chen, H.L., Lin, S.F., Xia, X.P., Long, X.P., 2007. Accretionary orogenesis of the Chinese Altai: insights from Paleozoic granitoids. Chem. Geol. 242, 22–39.
Zhang, C.L., Santosh, M., Zou, H.B., Xu, Y.G., Zhou, G., Dong, Y.G., Ding, R.F., Wang, H.Y., 2012. Revisiting the "Irtish tectonic belt": implications for the Paleozoic tectonic evolution of the Altai orogen. J. Asian Earth Sci. 52, 117–133.
Zhang, J., Sun, M., Schulmann, K., Zhao, G.C., Wu, Q.H., Jiang, Y.D., Guy, A., Wang, Y.J., 2015. Distinct deformational history of two contrasting tectonic domains in the Chinese Altai: their significance in understanding accretionary orogenic process. J. Struct. Geol. 73, 64–82.
Zhang, J.J., Wang, T., Tong, Y., Zhang, Z.C., Song, P., Zhang, L., Huang, H., Guo, L., Hou, Z.Q., 2017. Tracking deep ancient crustal components by xenocrystic/inherited zircons of Palaeozoic felsic igneous rocks from the Altai–East Junggar terrane and adjacent regions, western Central Asian Orogenic Belt and its tectonic significance. Int. Geol. Rev. 59, 2021–2040.
Zou, T.R., Chao, H.Z., Wu, B.Q., 1989. Orogenic and anorogenic granitoids in the Altay mountains of Xinjiang and their discrimination criteria. Acta Geol. Sin. Engl. Ed. 2, 45–64.

Further reading

Barker, F., 1979. Trondhjemite: Definition, environment and hypotheses of origin. In: Barker, F. (Ed.), Trondhjemites, dacites and related rocks. Elsevier, Amsterdam, pp. 1–12.